Rab8a regulates the exocyst-mediated kiss-and-run discharge of the *Dictyostelium* contractile vacuole

Miriam Essid[a,*], Navin Gopaldass[a], Kunito Yoshida[b], Christien Merrifield[b], and Thierry Soldati[a]
[a]Département de Biochimie, Faculté des Sciences, Université de Genève, Sciences II, CH-1211-Geneva 4, Switzerland;
[b]MRC Laboratory of Molecular Biology, Cambridge CB2 0QH, United Kingdom

ABSTRACT **Water expulsion by the contractile vacuole (CV) in *Dictyostelium* is carried out by a giant kiss-and-run focal exocytic event during which the two membranes are only transiently connected but do not completely merge. We present a molecular dissection of the GTPase Rab8a and the exocyst complex in tethering of the contractile vacuole to the plasma membrane, fusion, and final detachment. Right before discharge, the contractile vacuole bladder sequentially recruits Drainin, a Rab11a effector, Rab8a, the exocyst complex, and LvsA, a protein of the Chédiak–Higashi family. Rab8a recruitment precedes the nucleotide-dependent arrival of the exocyst to the bladder by a few seconds. A dominant-negative mutant of Rab8a strongly binds to the exocyst and prevents recruitment to the bladder, suggesting that a Rab8a guanine nucleotide exchange factor activity is associated with the complex. Absence of Drainin leads to overtethering and blocks fusion, whereas expression of constitutively active Rab8a allows fusion but blocks vacuole detachment from the plasma membrane, inducing complete fragmentation of tethered vacuoles. An indistinguishable phenotype is generated in cells lacking LvsA, implicating this protein in postfusion detethering. Of interest, overexpression of a constitutively active Rab8a mutant reverses the *lvsA*-null CV phenotype.**

Monitoring Editor
Patrick Brennwald
University of North Carolina

Received: Jun 27, 2011
Revised: Jan 9, 2012
Accepted: Feb 3, 2012

INTRODUCTION

Focal delivery of exocytic vesicles to specific domains of the plasma membrane (PM) is called focal exocytosis and is crucial for cell polarity, function, and fate. This process is used either for addition of bulk membrane or local delivery of specific cargo. It contributes to epithelial cell organization in apical and basolateral domains (Mellman and Nelson, 2008), to addition of membrane at the base of the phagocytic cup necessary for uptake of large particles (Groves *et al.*, 2008), or at the cell front for efficient cell motility (Spiczka and Yeaman, 2008). Focal exocytosis can occur either by full fusion, when the vesicle collapses into the PM, or by a kiss-and-run mechanism (Rizzoli and Jahn, 2007), when the vesicle forms a transient exocytic pore at the PM without membrane mixing (Tse *et al.*, 1993; Zimmerberg *et al.*, 1994). The exact mechanisms restricting fusion are unclear (Harata *et al.*, 2006).

Each step, from vesicle delivery to exocytosis and final pore closure, is highly regulated. The first contact between two membranes is defined as tethering that facilitates soluble *N*-ethylmaleimide–sensitive factor attachment protein receptor (SNARE) engagement and pore formation. Tethering is mediated by multisubunit protein complexes (Sztul and Lupashin, 2009), among which the exocyst complex is one of the best studied. The exocyst is an octameric complex of the subunits Sec3, Sec5, Sec6, Sec8, Sec10, Sec15, Exo70, and Exo84. It was first discovered in yeast (TerBush and Novick, 1995), where it tethers post-Golgi secretory vesicles to the PM to provide additional membrane material for cell wall biogenesis and bud growth. In mammalian cells, the exocyst is involved in focal exocytic processes, including neurite outgrowth, cytokinesis, various vesicular trafficking steps in polarized epithelial cells, and invasive cell motility (Hazuka *et al.*, 1999; Inoue *et al.*, 2003; Murthy *et al.*, 2003; Yeaman *et al.*, 2004; Spiczka

This article was published online ahead of print in MBoC in Press (http://www.molbiolcell.org/cgi/doi/10.1091/mbc.E11-06-0576) on February 9, 2012.

*Present address: Unité de Biologie des Interactions Cellulaires, Institut Pasteur, F-75015 Paris, France.

Address correspondence to: Thierry Soldati (thierry.soldati@unige.ch).

Abbreviations used: CA, constitutively active; CHS, Chédiak–Higashi syndrome; CV, contractile vacuole; DN, dominant negative; GAP, GTPase-activating protein; GEF, guanine nucleotide exchange factor; IP, immunoprecipitation; IRCM, interference reflection contrast microscopy; PM, plasma membrane; TIRFM, total internal reflection fluorescence microscopy; WT, wild type.

and Yeaman, 2008; Gromley *et al.*, 2005; Tsuboi *et al.*, 2005; Blankenship *et al.*, 2007; Chen *et al.*, 2007; Cascone *et al.*, 2008). In plants, the exocyst is involved in polarized secretion, pollen tube formation (Hala *et al.*, 2008), and cytokinesis (Fendrych *et al.*, 2010). In fungi, it has similar functions in hypha growth (Taheri-Talesh *et al.*, 2008).

Research on the exocyst has concentrated on its assembly and targeting to the PM. In yeast, delivery of the complex to the PM depends on the interaction of Sec15p with the small GTPase Sec4p (Guo *et al.*, 1999). Essential for targeting at the PM are Sec3p and Exo70p via interaction with the small GTPases Cdc42p, Rho1p, and Rho3p, as well as with phosphatidylinositol 4,5-bisphosphate (PI(4,5)P2; He *et al.*, 2007; Zhang *et al.*, 2008). Interference with any of the eight subunits blocks secretion and arrests growth. In mammalian cells, targeting works similarly. Exo70 interacts with $PI(4,5)P_2$ at the PM (Liu *et al.*, 2007). In contrast to yeast, however, mammalian Exo70 does not interact with Rho3 but does interact with TC10 (Inoue *et al.*, 2003). No major role has been proposed for Sec3, as it lacks a Rho-binding domain (Matern *et al.*, 2001). Sec15 interacts with Rab11-GTP on recycling endosomes (Zhang *et al.*, 2004) but not with the Sec4 homologue Rab8. Final assembly of the complex seems to take place at the PM. In yeast, transport of all subunits, except Sec3p and Exo70p, depend on the actin cytoskeleton (Boyd *et al.*, 2004). Studies in mammalian cells show two subcomplexes. RalA, a small GTPase that does not exist in yeast, regulates their assembly (Moskalenko *et al.*, 2003) into a rod-like structure (Hsu *et al.*, 1998).

Mechanisms of exocyst targeting and its involvement in focal exocytosis have been investigated in detail, but little is known about its possible role in kiss-and-run exocytosis and even less about mechanisms of tether dissociation or "detethering." In the present study, we used *Dictyostelium* as a model organism to address these questions. Membrane trafficking in *Dictyostelium* is similar to that in animal cells in both the secretory and endocytic pathways (Duhon and Cardelli, 2002; Neuhaus *et al.*, 2002). *Dictyostelium* possesses a further major organelle—the contractile vacuole (CV) system, a specialized osmoregulatory organelle found in freshwater protozoa and amoeba. In *Dictyostelium*, it consists of a dynamic network of interconnected membrane tubules and bladders. Under hypo-osmotic conditions, as water enters into the cytoplasm, H_3O^+ and HCO_3^- ions are pumped into the CV lumen. Following the osmotic gradient, water streams into the CV. When the CV bladder reaches its maximal diameter of 2–4 μm, it discharges its content through a pore at the PM (Heuser *et al.*, 1993) in a giant kiss-and-run process. Subsequently, CV and PM separate, and the empty CV bladder tubulates, fragments, and finally is reincorporated into the CV network. Cortical transport of the bladder and anchoring of the CV membrane in the cortical cytoskeleton are mediated by the class V myosin MyoJ (Jung *et al.*, 2009). The force that drives discharge and tubulation likely depends on the curvature-regulating function of MEGAP1, a Rho-GAP family protein with an F-BAR domain (Heath and Insall, 2008). A temperature-sensitive mutant of secA, the Sec1 orthologue, blocks CV discharge (Zanchi *et al.*, 2010), suggesting a parallel with exocyst-mediated exocytosis in yeast and mammalian cells.

The CV cycle is controlled by Rab proteins and their regulators. *Dictyostelium* has 52 Rab proteins (Weeks et al., 2005). For the vast majority of them, a human orthologue is clearly identified. Rab8a, 11a, 11c, and 14 have been localized to the CV (Bush *et al.*, 1994, 1996; Harris *et al.*, 2001; Du *et al.*, 2008). Of note, Rab8 and 11 regulate targeting of the exocyst to the PM in other systems. Disgorgin, a *Dictyostelium* homologue of the mouse Rab27a GTPase-activating protein (GAP; Reczek and Bretscher, 2001), was identified as a Rab8a GAP and functions in the CV cycle (Du *et al.*, 2008). Exposure of Disgorgin-knockout cells to low osmotic conditions results in strongly enlarged bladders that rapidly disappear after discharge (Du *et al.*, 2008), likely by fragmentation into numerous smaller structures that are prevented from reassembling in a bladder. Hydrolysis of GTP by Rab8a was suggested to be necessary for CV–PM fusion, and Rab8a was claimed to be an essential protein (Du *et al.*, 2008).

Drainin is a further conserved Rab-GAP like protein (with no measurable GAP activity) that regulates CV discharge (Gerisch *et al.*, 2002; Bos *et al.*, 2007; Du *et al.*, 2008). Drainin is recruited to the bladder in a Rab11a-GTP dependent manner shortly before discharge and remains during the whole process (Du *et al.*, 2008). Under hypo-osmotic conditions, the CV bladders of *drainin*-null cells become >10-fold larger than in wild-type cells. Instead of discharging, the bladder expands in close apposition to the PM. In these areas the membranes are tightly connected by a palisade-like structure closely resembling the "tethers" observed by Heuser (Figure 3 in Heuser, 2006). As a result of overinflation, abnormal CV discharge occurs explosively via rupture of the apposed membranes. Drainin might function as a volume sensor that signals to the palisade of spacers to prepare for pore formation and fusion (Becker *et al.*, 1999).

A further class of regulators of small GTPases associated with the CV function is made up of Rho-GDIs, as knockout of Rho-GDI1 or Rho-GDI2 leads to inflated CV bladders (Rivero *et al.*, 2002). Rho-GDI1 binds to Rac1a/b/c, RacB, RacC, and RacE, but none of them has been linked to the CV cycle. Besides small GTPases and their regulators, LvsA, a member of the family of Chédiak–Higashi syndrome (CHS) proteins, functions in CV discharge (Gerald *et al.*, 2002). CHS is a human autosomal disorder characterized by the presence of enlarged endolysosomal compartments. In certain cell types, this is associated with defects in the secretion of lysosomal hydrolases (Page *et al.*, 1998). The *Dictyostelium* homologues are called Lvs (large volume sphere) A–F (Kwak *et al.*, 1999). Green fluorescent protein (GFP)–LvsA labels the CV bladder when it reaches its maximal diameter and remains associated throughout the discharge phase until it concentrates in a very bright patch at the PM (Gerald *et al.*, 2002). No CV activity was detectable in *lvsA*-null cells. The CV network was fragmented into small punctae near the nucleus and at the cell periphery (Wu *et al.*, 2004). LvsA is proposed to preserve the structure of the CV during discharge and to play a role in pore closure (Du *et al.*, 2008) but its precise molecular function is unclear.

Although scattered morphological and molecular information about the process of CV discharge has been reported, the data suffer from a lack of integration and mechanistic understanding. In this study, we took advantage of the inducible, easily observable process of CV discharge to study the function of the exocyst and its regulators in kiss-and-run focal exocytosis. We describe a molecular cascade that drives the entire process from targeting the bladder to the PM to pore closure and bladder detachment from the PM. Our major finding is that the exocyst complex, together with the essential protein Rab8a, plays a role in focal exocytosis by the kiss-and-run mechanism. We present evidence that CV-associated Rab8a is activated by a guanine nucleotide exchange factor (GEF) activity associated with the exocyst complex that acts at the time of its recruitment onto the CV bladder. In addition, we propose a new role for a CHS protein in "detethering" a vacuole from its target membrane after fusion, shedding more light on this mysterious protein family.

RESULTS

Interfering with Rab8a function alters CV morphology and its discharge cycle

As described earlier, ablation of the Disgorgin gene encoding a Rab8a GAP resulted in a prominent CV discharge defect, but the

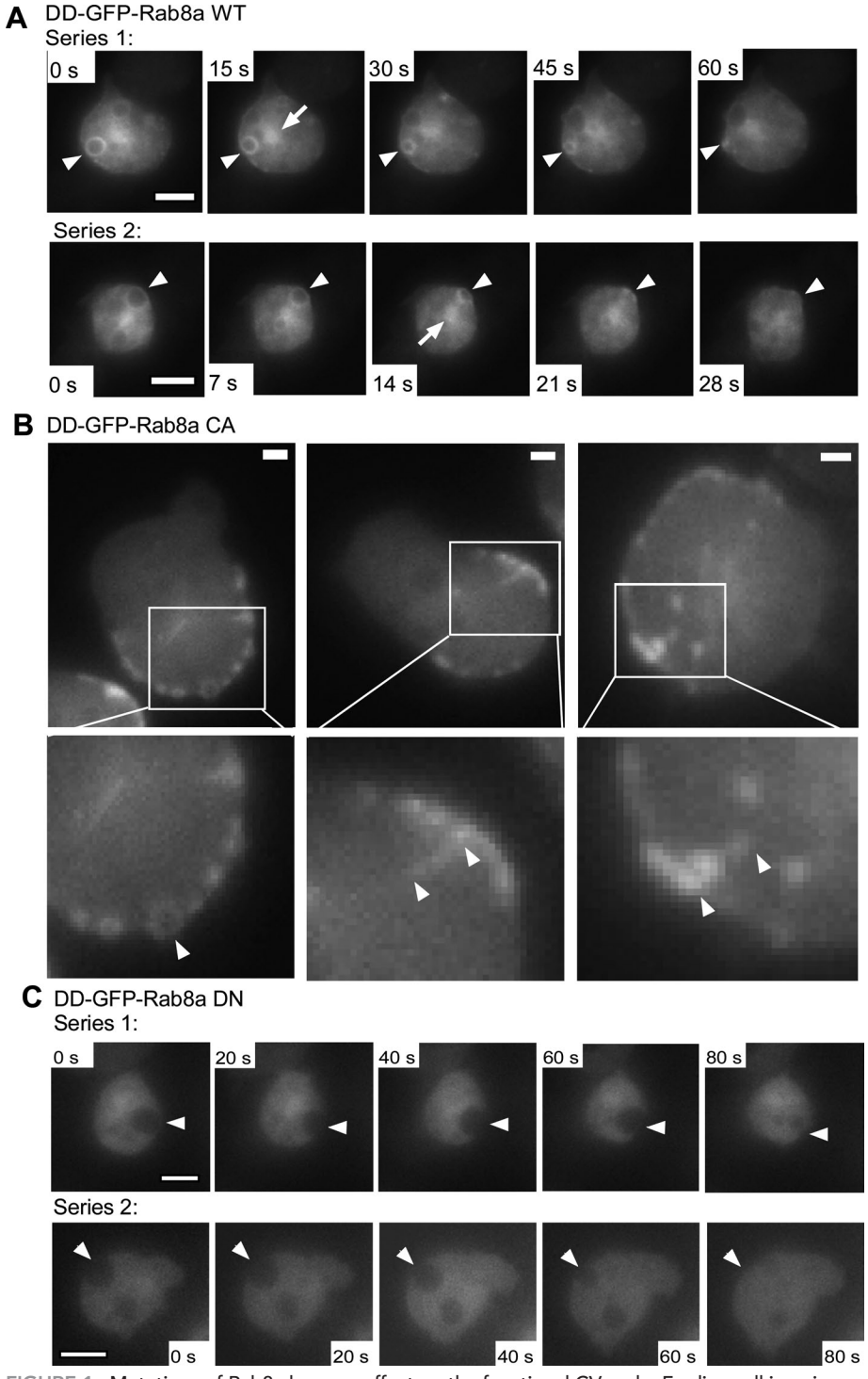

FIGURE 1: Mutations of Rab8a have an effect on the functional CV cycle. For live-cell imaging by widefield microscopy, cells were incubated for 30 min with HL5c medium diluted 1:2 with water and imaged. (A) DD-GFP-Rab8a WT was recruited to CV bladder shortly before discharge and remained until completion (arrowhead); series 1, 60 s (Supplemental Movie S2), and series 2, 28 s (Supplemental Movie S3). Rab8a WT was also in a juxtanuclear region (arrow). (B) DD-GFP-Rab8a CA localized to small vesicles at PM and tubules and vesicles that move bidirectionally between PM and cell center (arrowhead). Bottom, magnification of areas in top (Supplemental Movie S4, right image; Supplemental Movie S5, left image). (C) DD-GFP-Rab8a DN appeared cytosolic. Arrowheads point to exocytic-like events. The discharge process was slowed down (Supplemental Movies S6 and S7, 80 s). Scale bars, 5 μm.

cells were viable (Du *et al.*, 2008). The authors reported their failure at generating a Rab8a knockout, indicating a role for Rab8a not restricted to the CV cycle. Therefore we expressed dominant mutant forms of Rab8a in a strictly regulated manner by adapting to *Dictyostelium* a co/posttranslational degradation system (Banaszynski *et al.*, 2006). In brief, Rab8a is fused at the C-terminus of the destabilizing domain (DD). On translation, the DD domain causes rapid degradation of the DD fusion protein, but addition of the compound Shield-1 rapidly and reversibly stabilizes it (Supplemental Figure S1 and Supplemental Movie S1), allowing us to observe direct and acute effects of Rab8a mutant expression. Fusion of DD-GFP or monomeric red fluorescent protein (mRFP; Supplemental Figure S2) to the N-terminus of Rab8A did not alter its localization to the CV (Du *et al.*, 2008). Both colocalized with the CV markers VatA (Neuhaus *et al.*, 1998), a subunit of the vacuolar H^+-ATPase (V-ATPase; Supplemental Figure S2, A and B, arrowheads) and calmodulin (CaM, Supplemental Figure S2C, arrowhead; Zhu and Clarke, 1992) on large CV bladders in close proximity to the PM. Some CV bladders deeper inside the cell were Rab8a negative but VatA positive (Supplemental Figure S2A, arrow) and CaM positive (Supplemental Figure S2C, arrow), indicating transient association of Rab8a with the CV. The remaining structures are endosomes, known to be VatA positive but CaM negative (see, e.g., Figure 2A, asterisk, later in the paper). Live-cell imaging (Supplemental Movies S2 and S3) confirmed CV localization and showed that mRFP/GFP-Rab8a and DD-GFP-Rab8a (Figure 1A, arrow) also localized to the juxtanuclear region. This area corresponds to pericentriolar recycling endosomes (Charette *et al.*, 2006) and Golgi, possibly indicative of CV-independent functions of Rab8a. Recruitment of DD-GFP-Rab8a wild type (WT) to the CV was temporally regulated. It appeared at the CV bladder shortly before it reached its maximal diameter and stayed on the contracting bladder during the entire discharge process, finally remaining as a patch at the PM (Figure 1A, arrowheads). Because DD-GFP tagging did not affect the specific recruitment of Rab8a WT, we used that system to express Rab8a mutants that are predicted to interfere with its functional cycle, by locking them in their GTP-bound, constitutively active (Q74L = CA) or nucleotide-free, dominant negative (N128I = DN) form (Powell and Temesvari, 2004). Similar to Rab8a WT, DD-GFP-Rab8a CA labeled a few vesicles in the cell center, but it mainly localized to a large pool of small vesicles at the cell periphery (Figure 1B). The latter vesicles were densely packed at one pole of the cell, forming a hemispherical cap closely apposed to the PM. Tubules and vesicles connected the two populations by bidirectional movement, probably along microtubules (Supplemental Movies S4 and S5). In

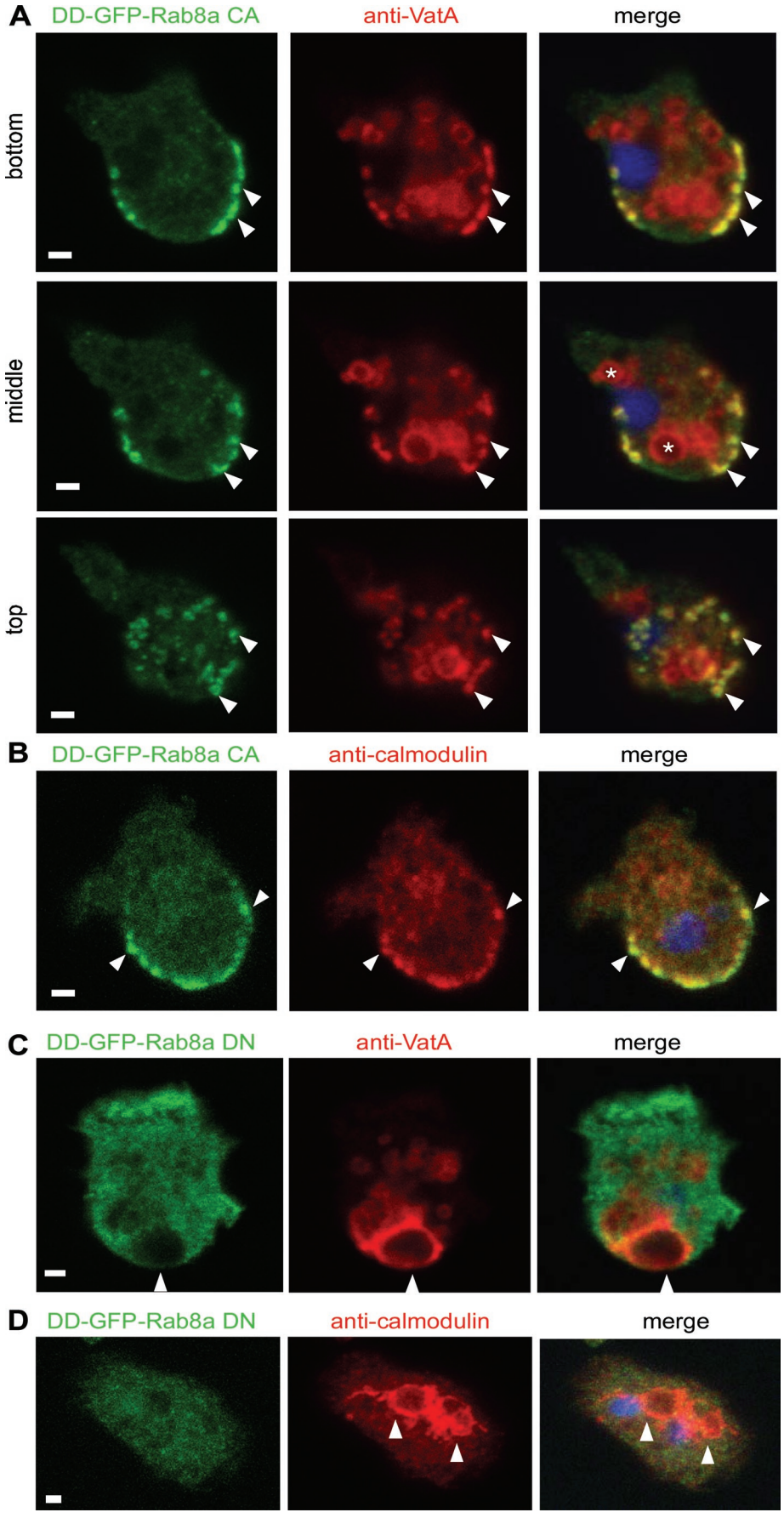

FIGURE 2: Mutations in Rab8a induce changes in the morphology of the CV system. Cells overexpressing DD-GFP-Rab8a CA (A, B) or DD-GFP-Rab8a DN (C, D) were treated as in Figure 1, fixed, and labeled for VatA (A, C) or CaM (B, D). (A) The cell is shown in *x*, *y* sections from bottom to top. DD-GFP-Rab8a CA and VatA colocalize at vesicles beneath PM (arrowhead), forming a crescent in transverse sections (bottom, middle) and discrete rings in a tangential section (top). VatA localized also to endosomes (asterisks). (B) DD-GFP-Rab8a CA colocalized at similar structures with CaM (arrowhead). (C, D) DD-GFP-Rab8a DN appeared cytosolic, but the CV system seemed intact. (C) VatA-labeled large CV bladder (arrowhead). (D) Calmodulin-labeled CV network, including bladders (arrowhead). Scale bars, 1 μm.

fixed cells, these DD-GFP-Rab8a CA-positive structures colocalized at the cell periphery with VatA (Figure 2A) and CaM (Figure 2B), establishing their identity as part of the CV system. Serial *x*, *y* sections at various positions through the cell clearly showed that the collapsed crescent shape seen at bottom and mid-height was formed by the accretion of small individual vesicles at the PM (Figure 2A, arrowheads), as best observed in tangential sections at the top of the cell. These "mini-CV bladders" were nevertheless functional, as discharge events were observed (Figure 1B, left, and Supplemental Movies S4 and S5). In contrast to the WT and CA forms, DD-GFP-Rab8a DN appeared entirely cytosolic (Figures 1C and 2, C and D). Nevertheless, live imaging revealed exocytic events strongly reminiscent of CV bladder discharge (Supplemental Movies S6 and S7), even though the average duration of the events was twofold longer than in wild-type cells or cells expressing DD-GFP-Rab8a WT (compare the time stamps in Figure 1, A and C). The CV function appears to be not completely abrogated, likely because of basal expression of endogenous Rab8a. Labeling for VatA and CaM showed that cells expressing DD-GFP-Rab8a DN possessed an apparently normal CV system with inflated CV bladders (Figure 2C) and CV network (Figure 2D). To assess more quantitatively the effect of DD-GFP-Rab8a DN overexpression, we counted the number of CV bladders per cell and measured their size. To this purpose, Ax2, DD-GFP-Rab8a WT, and DD-GFP-Rab8a DN cells were stained for CaM and analyzed with ImageJ. About 70% of DD-GFP-Rab8a DN cells had two or more CV bladders, whereas this was only the case for <30% of Ax2 and DD-GFP-Rab8a WT cells. Greater than 70% of Ax2 and DD-GFP-Rab8a WT cells had one or no CV bladder (Supplemental Figure S1D). The maximal diameter of CV bladders was also affected (Supplemental Figure S1E). Compared to wild-type cells, the diameter of CV bladders in most

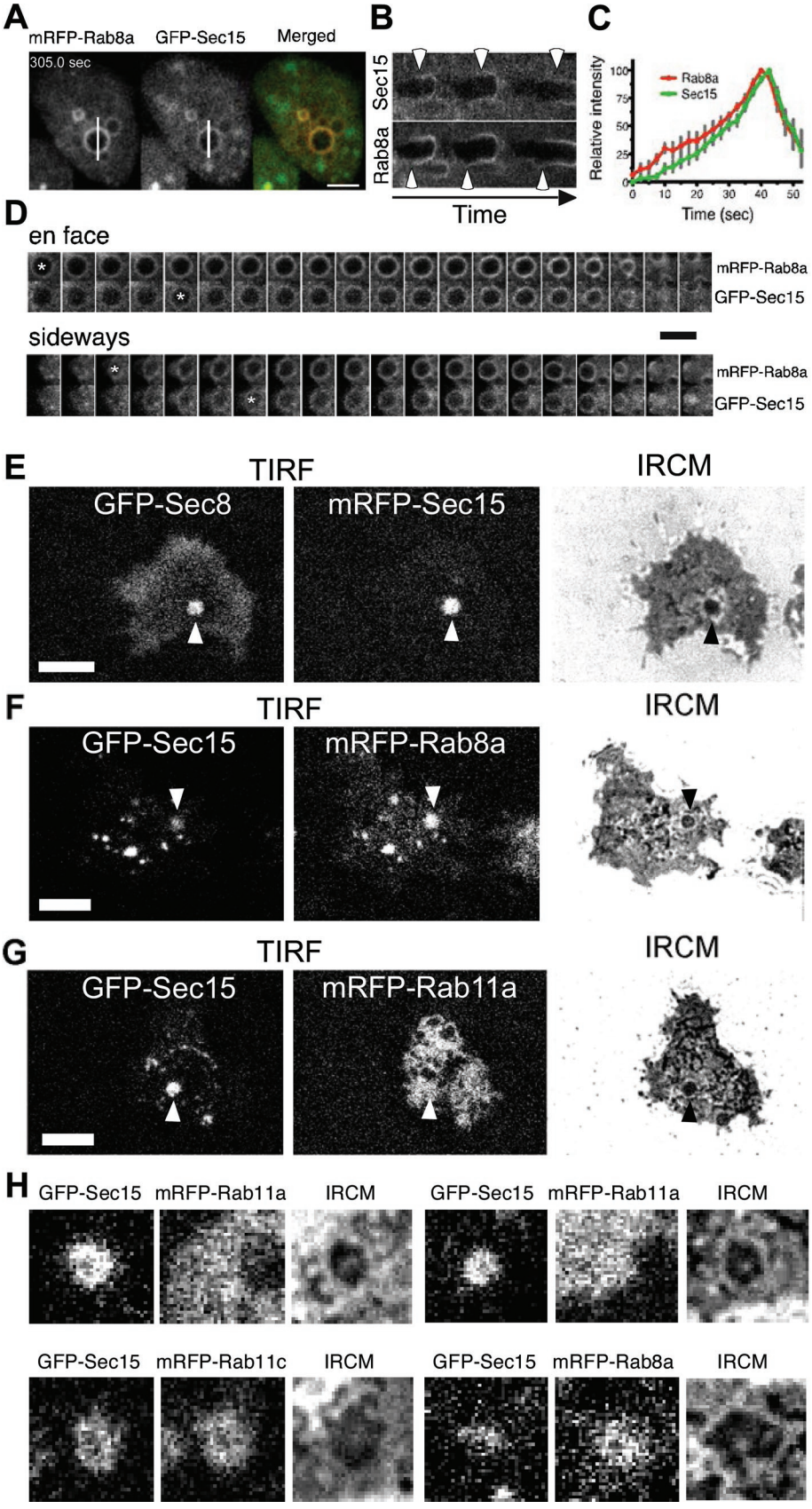

FIGURE 3: The exocyst concentrates at CV–PM contact sites during discharge. For live imaging with a spinning disk confocal microscope, cells were placed in LoFlo medium diluted 1:2 with water and imaged. (A) Snapshot of Supplemental Movie S8, showing a cell expressing GFP-Sec15/mRFP-Rab8a. The white line corresponds to the *y*-axis of the kymograph in B. Scale bar, 5 µm. (B) Kymograph of three CV discharge events from Supplemental Movie S8, with images (and line scan) taken every 2.5 s. White arrowheads indicate the time of first appearance of the corresponding protein over background. (C) Quantification of the relative fluorescence signals of GFP-Sec15 and mRFP-Rab8a during six discharge events of similar size and duration. (D) Galleries showing two discharge events from an "en face" (upper) or sideways (lower) view. Asterisks indicate first time of recruitment of the corresponding proteins. Interval between two frames is 2.5 s. Each frame is 5 µm wide. (E–G) Cells expressing GFP-Sec8/mRFP-Sec15 (E; Supplemental Movie S9), GFP-Sec15/mRFP-Rab8a (F; Supplemental Movie S10), or GFP-Sec15/mRFP-Rab11a (G; Supplemental Movie S11) were imaged by TIRFM/IRCM. The darkest areas of the IRCM image define places of discharge, where GFP-Sec8/mRFP-Sec15 (E) and GFP-Sec15/mRFP-Rab8a (F) colocalized (arrowhead). (G) mRFP-Rab11a was evenly distributed over the network, whereas GFP-Sec15 localized (arrowhead) to dark areas of the IRCM image. (H) Zooms on examples of discharge sites where the center of the fluorescent area is darker and corresponds to a brighter zone in IRCM. Scale bars, 5 µm.

DD-GFP-Rab8a DN–expressing cells was significantly larger. In cells with one bladder it resulted in a doubling of bladder volume. Expression of DD-GFP-Rab8a WT affected CV size, but only significantly in cells with three or more bladders. These data suggest that expression of DD-GFP-Rab8a DN severely prolongs the CV cycle, resulting in cells with more and larger CV bladders. We conclude that Rab8a CA induces CV structures that are fragmented and tightly associated with the PM, whereas Rab8a DN induces larger CV bladders because of an inefficient discharge process. The opposite phenotypes of Rab8a CA and DN suggested a role for Rab8a in regulating the efficiency of membrane docking, tethering, and/or fusion. We hypothesized that Rab8a regulates CV–PM tethering via the exocyst complex, a known effector of Sec4 (the yeast Rab8a orthologue).

The exocyst complex localizes to Rab8a-positive CV bladders during discharge

Live-cell imaging showed that the exocyst subunit GFP-Sec15 was partly cytosolic and was recruited to preexisting large mRFP-Rab8a–positive vacuoles. Supplemental Movie S8 shows multiple examples of discharge events that are visible either in an "en face" manner and others that occur sideways. The former became visible as ring structures (Figure 3D, top, and Supplemental Movie S8) and the latter as rings, patches,

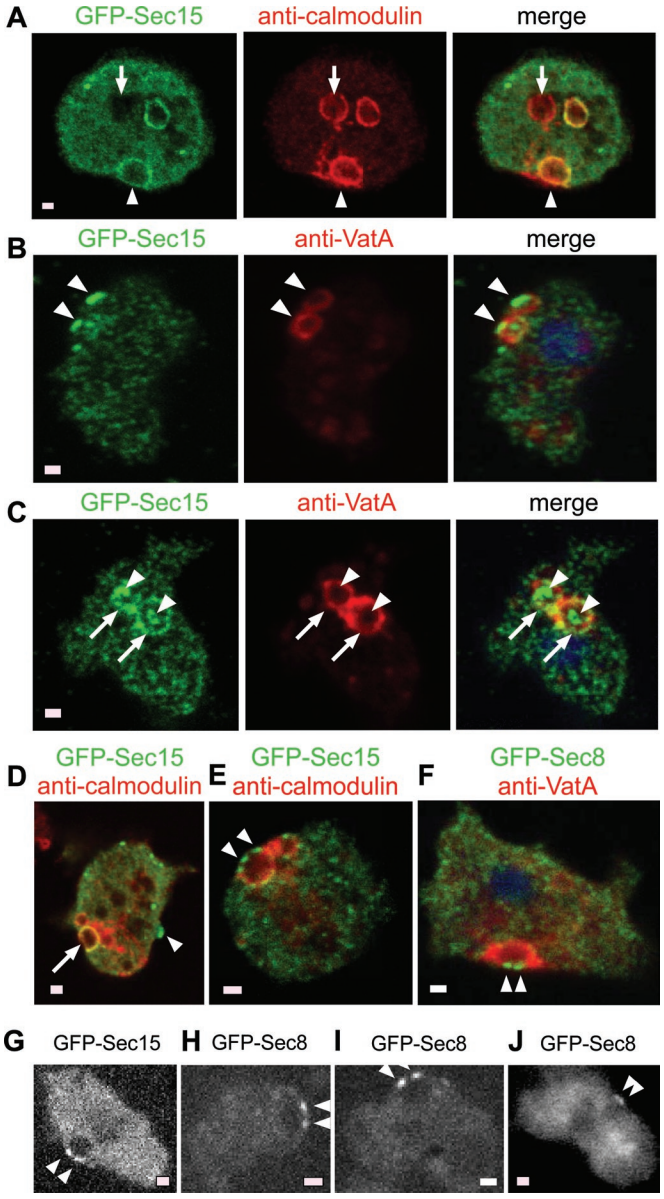

FIGURE 4: The exocyst localizes to CV bladders during discharge. Cells overexpressing GFP-Sec15 (A–E) or GFP-Sec8 (F) were treated as in Figure 1, fixed, and labeled for VatA (B, C, F) or CaM (A, D, E). (A) GFP-Sec15 localized to a subset of CaM-positive bladders (arrowhead), whereas some were negative (arrow). (B, C) GFP-Sec15 localized in patches to CV–PM contact sites in transverse sections (B, arrowhead), and to two rings in tangential sections (C), of which only the outer is VatA positive (arrow). The inner ring might be the zone surrounding the pore (arrowhead). (D) GFP-Sec15 localized to whole bladders (arrow) and to patches and cellular protrusions (arrowhead). (E, F) GFP-Sec15 and GFP-Sec8 localized in a doublet of patches at discharge sites (arrowhead). (G–J) Examples of localization of the exocyst at "lip" patches from time-lapse movies taken with a spinning disk confocal microscope. Scale bars, 1 μm.

and dots (Figure 3D, bottom, and Supplemental Movie S8). Rab8a was recruited before Sec15, as indicated by comparing their time of appearance around vacuoles (Figure 3D) and by monitoring their respective intensities along a line scan as a function of time (Figure 3B, kymographs). Quantification of six discharge events of similar size and duration revealed a lag of up to 10 s, followed by very similar rises, peaks, and disappearances (Figure 3C). The Rab8a/Sec15–positive structures of discharge events visualized sideways (Figure 3D, bottom, and Supplemental Movie S8) sometimes looked like two "lips" around a central darker area where the discharge occurred, until they coalesced into a single, slightly protruding patch (see also Figure 4, D–F) that vanished in a matter of seconds to a minute. A gallery of such lip structures, from time-lapse movies taken with a spinning-disk confocal microscope, is shown in Figure 4, G–J, demonstrating that they are not fixation artifacts.

To increase the spatial and temporal resolution of the observation, we used a combination of total internal reflection fluorescence microscopy (TIRFM) and interference reflection contrast microscopy (IRCM). The tight apposition of CV and PM at exocytic sites gives rise to dark areas in IRCM (Figure 3, E–G, arrowheads; Heuser, 2006). The localization of the exocyst between CV and PM in close proximity to the glass interface gave rise to bright signals coinciding with the IRCM dark signature (Figure 3, E–G, arrowheads). In a cell line coexpressing GFP-Sec8 and mRFP-Sec15, both largely colocalized at the bladders during the whole discharge process (Figure 3E and Supplemental Movie S9). The same was observed in a cell line coexpressing GFP-Sec15 and mRFP-Rab8a (Figure 3F and Supplemental Movie S10). This contrasted with mRFP-Rab11a, which was evenly distributed over the entire CV system, neither enriched nor excluded from places of CV discharge (Figure 3G and Supplemental Movie S11). We made similar observations with Rab11c. These results strongly emphasize the specificity of the Sec15-Rab8a colocalization. Moreover, in many instances, the center of the bright Sec8, Sec15, or Rab8a areas were darker, as if excluded from a zone brighter in IRCM and likely corresponding to the pore (Figure 3H). We conclude that Rab8a, and Sec8/Sec15 are recruited sequentially to the fully inflated CV bladders shortly before discharge and continue to line the exocytic pore until completion of the process.

Observations on fixed cells confirmed GFP-Sec8 and GFP-Sec15 localization at the CV bladder. The exocyst subunits decorated the surface of spherical bladder structures that appeared as rings in many confocal sections, colocalizing with VatA and CaM (Figure 4, A, C, and D). In some sections across the site where the discharging CV contacted the PM, the staining appeared as patches or doublet of dots (Figure 4, B, E, and F). In a few striking cases, the exocytic site was observed in an "en face" view, revealing details of the exocyst arrangement. When the section is tangential to the plane of contact between the CV bladder and the PM, GFP-Sec15 localizes to two concentric rings (Figure 4C). We propose that the outer circle represents the projection of the outline of the VatA-positive CV bladder membrane, and the inner circle represents the outline of the pore. We conclude that the different localizations shown in Figure 4 are snapshots from the temporal series of events shown in Supplemental Movie S8 and quantitated in Figure 3, A–D.

We suggest that the structures observed by Heuser (see Figure 3 in Heuser, 2006) and Becker and colleagues (see Figure 3 in Becker *et al.*, 1999) at the site of contact between CV and PM correspond to the exocyst. In support of this claim, the length measured for this palisade or picket fence was estimated between 15 and 30 nm, in perfect agreement with the dimension of the exocyst complex estimated to between 10 and 30 nm by negative-stain electron microscopy (Hsu *et al.*, 1998; Munson and Novick, 2006). Taken together, these results not only confirm our hypothesis that the exocyst is involved in CV discharge, but they also suggest that the complex assembles and interacts directly with Rab8a.

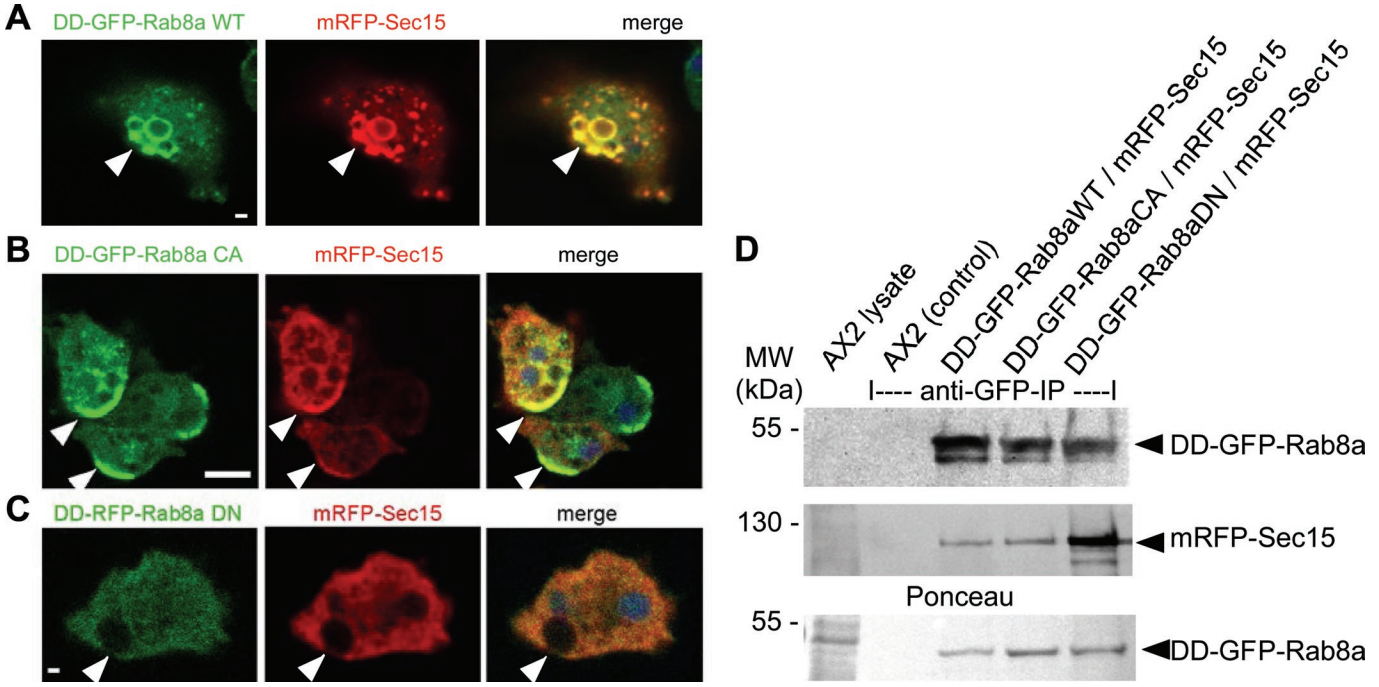

FIGURE 5: Recruitment of the exocyst to the CV bladder depends on Rab8a-GTP. Cells overexpressing DD-GFP-Rab8a WT, CA, or DN and mRFP-Sec15 were treated as in Figure 1 and either prepared for immunofluorescence or used for anti-GFP IP. (A) DD-GFP-Rab8a WT and mRFP-Sec15 colocalized on CV bladders. (B) DD-GFP-Rab8a CA and mRFP-Sec15 colocalized on peripheral CV-derived vesicles. (C) DD-GFP-Rab8a DN and mRFP-Sec15 appeared cytosolic. Scale bars, 1 μm (A, C), 5 μm (B). (D) Immunoblot of GFP-Trap IPs with whole-cell lysates from mutant cell lines. Ax2 cells were used as negative control. The lysate volumes were adjusted so as to precipitate similar amounts of GFP-Rab8a. Blots were probed with anti-GFP (top) or anti-mRFP (middle) antibodies. Bottom, a Ponceau S staining used as a loading control. Molecular weights are indicated on the left.

Rab8a-GTP recruits the exocyst to the contractile vacuole

To further address the question of a potential Rab8a–Sec15 effector relationship, we assessed the effect of Rab8a mutations on the localization of Sec15 in cell lines stably coexpressing DD-GFP-Rab8a WT, CA, or DN and mRFP-Sec15. As expected from their individual localizations (Supplemental Figure S2 and Figures 2 and 4), DD-GFP-Rab8a WT and mRFP-Sec15 perfectly colocalized at CV bladders (Figure 5A). Expression of DD-GFP-Rab8a CA changed neither the membrane identity of the CV-derived vesicles nor the specific recruitment of mRFP-Sec15. Both DD-GFP-Rab8a CA and mRFP-Sec15 colocalized at the small, peripheral, CV-derived vesicles aggregated at the hemispherical cap (Figure 5B). In DD-GFP-Rab8a DN–expressing cells, the localization of mRFP-Sec15 at the CV bladder was lost (Figure 5C), and both proteins appeared cytosolic. Therefore recruitment of Sec15 to the CV bladder membrane depends on Rab8a in its GTP-bound form, but Western blot of anti-GFP immunoprecipitates (IPs) revealed that mRFP-Sec15 interacted with all three forms of Rab8a (Figure 5D). When normalized to the amount of immunoprecipitated GFP-Rab8a, about five times more mRFP-Sec15 was pulled down with DD-GFP-Rab8a DN than with DD-GFP-Rab8a WT or CA. Trapping of the exocyst complex by the DN form of Rab8a suggests that it normally acts as a GEF for Rab8a and not strictly as an effector. We propose that Rab8a first associates with the CV in its GDP-bound form seconds before it recruits the exocyst complex concomitant with catalyzed exchange of GDP for GTP. Recruitment of both is lost in Rab8a DN–expressing cells because the cytosolic, nucleotide-free Rab8a scavenges and blocks the exocyst-associated GEF and thus hinders its CV recruitment.

Identification of novel exocyst interaction partners acting in CV discharge

To further dissect the function of the exocyst, we made several (unsuccessful) attempts to knock out the sec15 gene, strongly indicating that, like Rab8a, the exocyst is essential. As an alternative, we chose to identify exocyst interaction partners using Y2H screens with full-length Sec15 (Supplemental Table S1A) and with the C-terminal half of Exo70 (Exo70-C; Supplemental Table S1B), as well as using anti-GFP IPs (Supplemental Table S1C). For proteomic analyses, the samples from two separate IP experiments were separated by SDS–PAGE and either stained with colloidal Coomassie (Figure 6D) or silver (Supplemental Figure S3), cut into slices, and analyzed by liquid chromatography–tandem mass spectrometry (LC-MS/MS). The results of the Y2H and IP/MS screens can be separated into three categories. The most relevant proteins with highly significant Hybrigenics or Mascot scores are listed in Supplemental Table S1, A–C.

First, we identified a series of interacting partners from a subset of membrane-trafficking pathways that are briefly mentioned in the *Discussion*. We believe that involvement of the exocyst in tethering events besides its involvement in CV discharge accounts for its essentiality.

Second, we obtained confirmations for some direct/indirect interactions between the exocyst subunits themselves. First, because Sec8 and Sec15 do not interact directly in the octameric complex, assembly of tagged subunits was verified by coIP performed with a cell line overexpressing GFP-Sec8 and mRFP-Sec15 (Figure 6A). Then IPs from GFP-Sec8– or GFP-Sec15–expressing cells confirmed coassembly of tagged and endogenous subunits and suggested

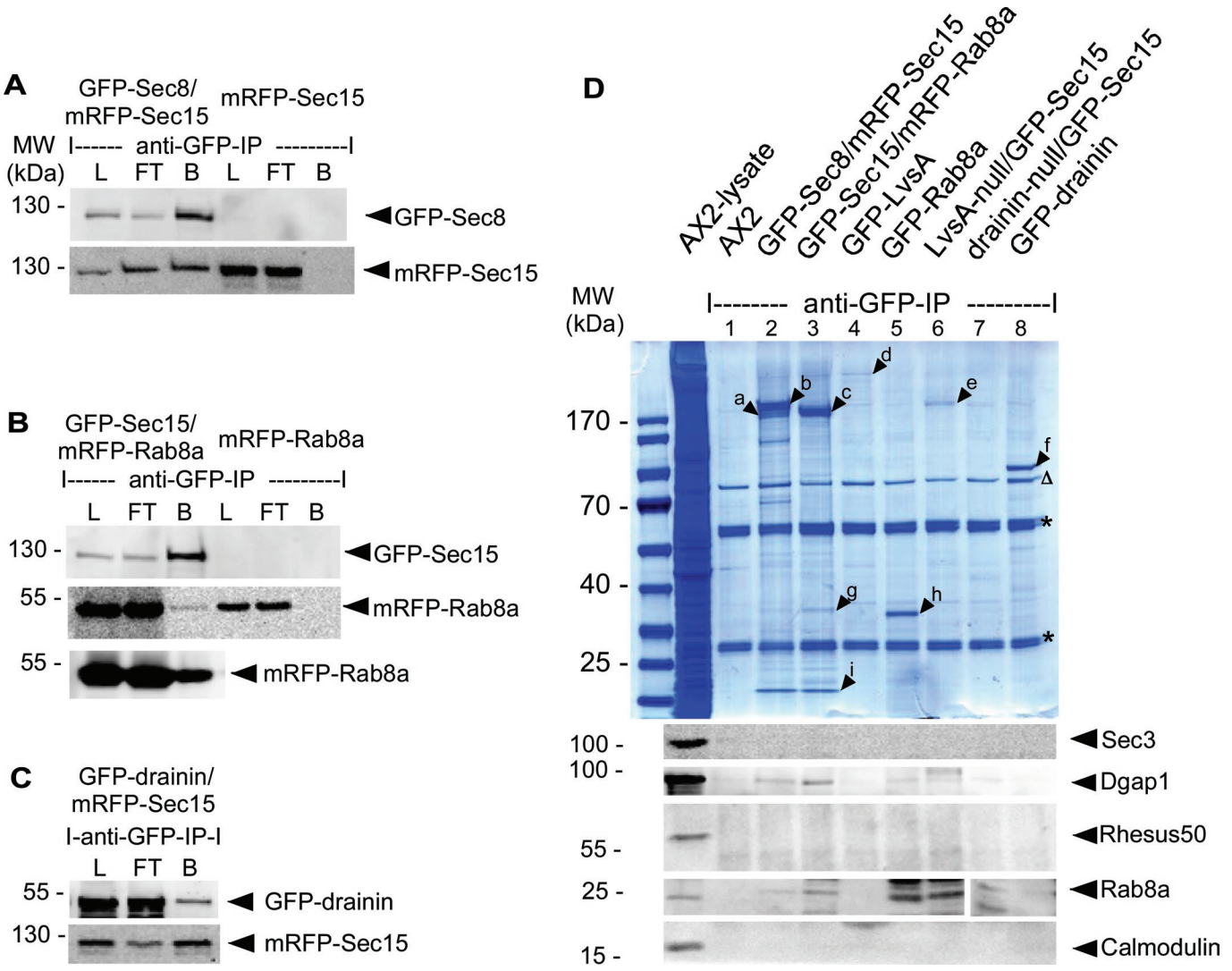

FIGURE 6: Identification of exocyst interaction partners by IP. Analysis of anti-GFP IPs from the cell lines indicated at the top by Western blot and MS. (A–C) Western blots. B, beads; FT, flowthrough; L, lysate. After anti-GFP IPs, two gels were run in parallel, and one was Coomassie stained (D),and one silver stained; they were cut into individual slices and analyzed by LC-MS/MS (Supplemental Figure S2). The Ax2 cells served as negative control. Arrowheads point to bands corresponding to overexpressed proteins: a, mRFP-Sec15; b, GFP-Sec8; c, GFP-Sec15; d, GFP-LvsA; e, GFP-Sec15; f, GFP-Drainin. Arrowheads in g–i mark specific proteins that could not be identified, and Δ indicates a contaminant of unknown identity. Asterisks mark heavy and light chain of IP antibodies. Bottom, immunoblots on the same IP samples. Molecular weights are indicated on the left and detected antigens on the right (arrowheads).

that in *Dictyostelium* the exocyst might be subdivided into two subcomplexes. Indeed, five of the eight exocyst subunits—Sec6, Sec8, Sec10, Sec15, and Exo70—were identified by IP/MS and likely belong to one subcomplex. Sec3, despite being identified in the Exo70-C Y2H screen, was absent from all the IPs (Figure 6D) and might thus belong to a second subcomplex. Moreover, GFP-Sec15 coprecipitated with mRFP-Rab8a (Figure 6B), and anti-Rab8a Western blot identified endogenous Rab8a in every IP from Sec15-overexpressing cells (Figure 6D), confirming the interaction of the Rab8a constructs with Sec15.

Third and most important, we identified novel partners for the exocyst that are likely linked to its CV-tethering functions. In the Y2H screen with Sec15 and Exo70-C, we identified subunits of the V-ATPase, VatA, and VatE, respectively (Supplemental Table S1, A and B). Confirming these hits, IP/MS from stable cell lines expressing combinations of GFP-Sec8 or GFP-Sec15 with mRFP-Sec15 or mRFP-Rab8a also identified five of the V-ATPase subunits—VatA, B, C, D, and M (Supplemental Table S1C). Absence of other abundant CV proteins from the IP/MS, such as Rhesus 50 (Benghezal *et al.*, 2001) and CaM (Figure 6D), excludes unspecific interaction with the very abundant V-ATPase. Interaction of the exocyst with the V-ATPase might be of great mechanistic importance to specify the recruitment of the activated complex to the CV before discharge. Of interest, VatA was found in complex with Disgorgin (Du *et al.*, 2008).

Huntingtin was also identified as a high-confidence Y2H interactor of both Sec15 and Exo70, possibly offering a mechanistic background to the recent observation that *Huntingtin*-null *Dictyostelium* cells appear to be extremely osmosensitive (Myre *et al.*, 2011). However, the most interesting Y2H hit with Sec15 was LvsA, a Chédiak–Higashi–related protein of the BEACH family already involved in CV bladder discharge (Du *et al.*, 2008). Most important, anti-GFP IPs

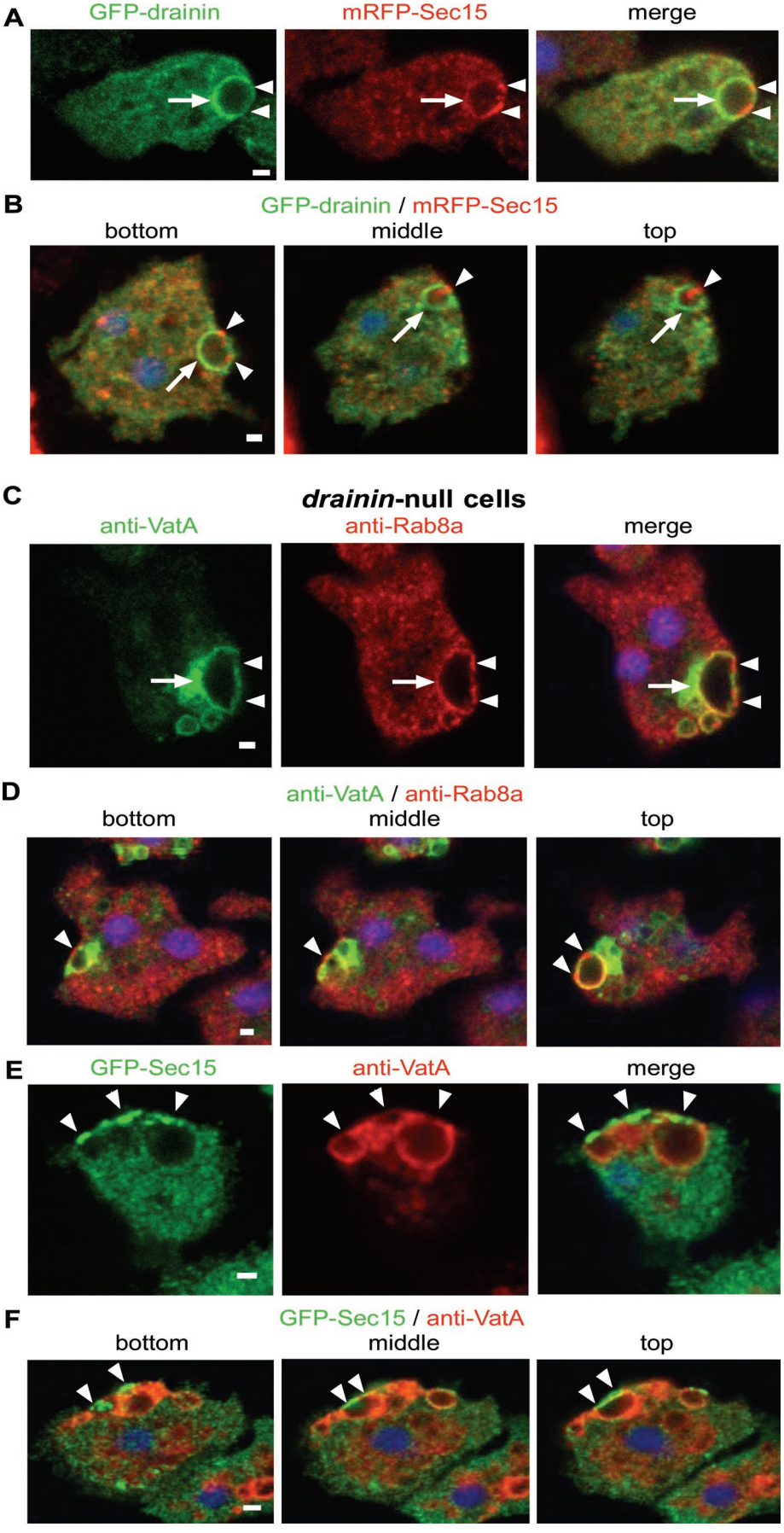

from stable cell lines expressing GFP-LvsA revealed association with endogenous Sec8 and Sec15 (Supplemental Table S1C), confirming the Y2H results and strengthening the possibility that they might act together in the CV cycle. We also included a GFP-Drainin–expressing cell line because of its reported role in CV bladder discharge (Becker *et al.*, 1999; Du *et al.*, 2008). It is remarkable that anti-GFP IPs from cells expressing GFP-Drainin and mRFP-Sec15 followed by Western blot revealed that Drainin and the exocyst interact in vivo (Figure 6C). To assess whether genetically interfering with CV-discharge affects the spectrum of Sec15-binding partners, we generated *lvsA*-null and *drainin*-null cell lines overexpressing Sec15. In these cases, anti-GFP IP/MS failed to detect the exocyst interactors identified in functional conditions.

Finally, Rac1a was also detected by both Y2H (Supplemental Table S1B) and IP/MS (Supplemental Table S1C) approaches and might be one of the small GTPases that regulate exocyst anchoring at the PM. This hypothesis is strengthened by identification of DGAP1, a known Rac1a-interacting protein and regulator, in some of the exocyst IPs (Figure 6D and Supplemental Table S1C).

Drainin regulates the commitment to pore formation for CV discharge

GFP-Drainin and mRFP-Sec15 were both found on the CV bladders in contact with the PM, but, whereas GFP-Drainin was enriched at the back of the bladder, mRFP-Sec15 concentrated in dots and small patches at the bladder-PM contact sites (Figure 7, A and B). Of interest, the CV marker VatA was also partially excluded from the contact sites, possibly as a consequence of a safeguard mechanism that prevents diffusional spilling at the PM after

FIGURE 7: Drainin is essential for correct localization of the exocyst, and Rab8a for CV discharge. Cells were treated as in Figure 1, fixed, and labeled with indicated antibodies. (A, B) GFP-Drainin and mRFP-Sec15 colocalized, but GFP-Drainin localized more prominently to the back of discharging CV bladder (arrow), whereas mRFP-Sec15 concentrated in lips at places of CV–PM contact (arrowheads). (C–F) *Drainin*-null cells exhibited large, VatA-positive CV bladders, tightly connected to PM. Rab8a localized to CV–PM contact zones in large patches (C, D, arrowhead). GFP-Sec15 strongly accumulated at enlarged CV–PM contact zones (E, F, arrowhead). Scale bars, 1 μm.

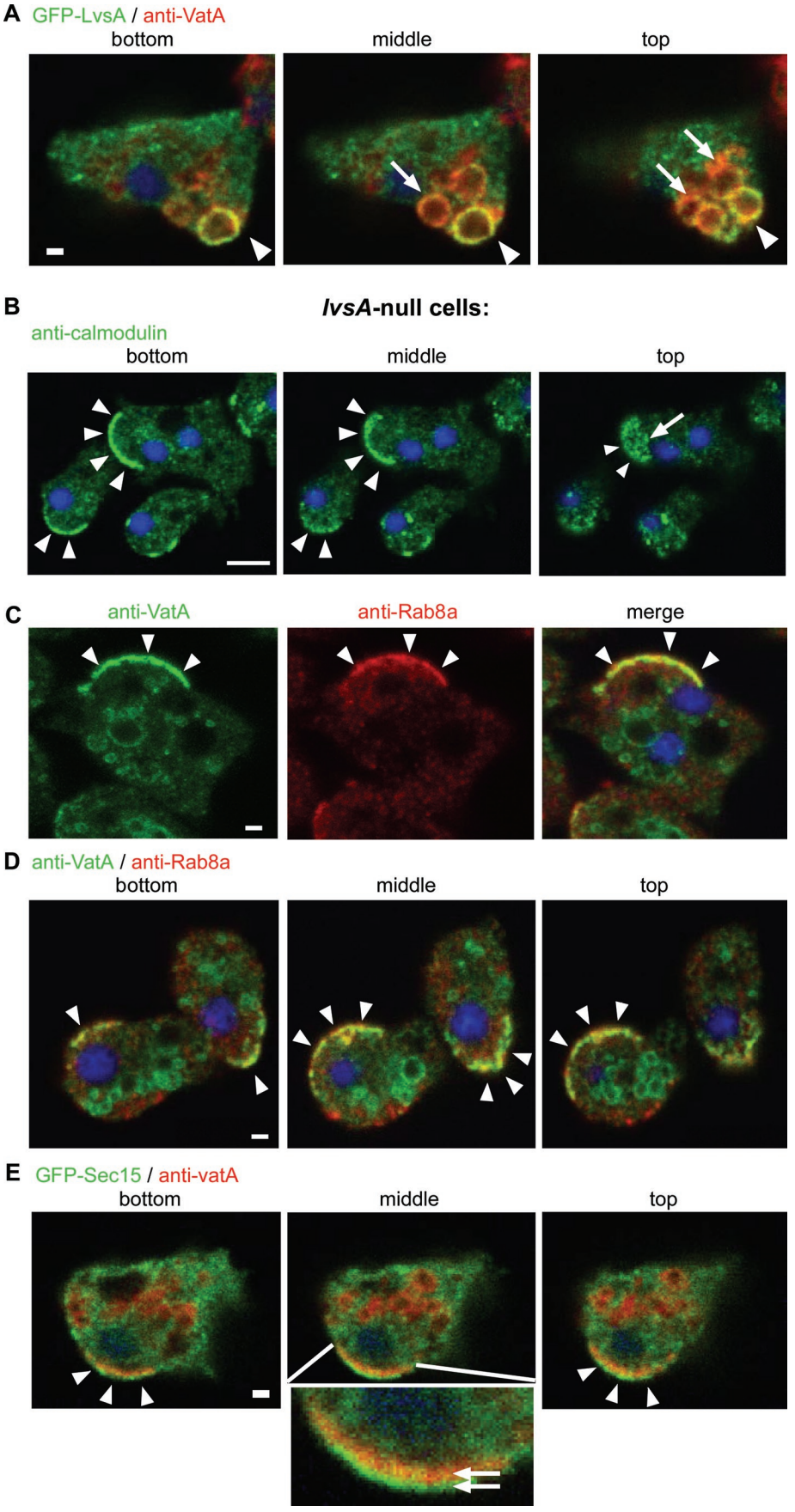

FIGURE 8: LvsA is involved in detethering of CV bladders after discharge. Cells were treated as in Figure 1, fixed, and labeled for VatA. (A) The *x*, *y* confocal sections from bottom to top of the cell. All the CV bladders were VatA positive (arrow), but only those close to PM were additionally GFP-LvsA-positive (arrowhead). (B) In *lvsA*-null cells CV bladders were fragmented and collapsed against PM, forming a VatA-positive crescent in tangential sections (arrowheads). Transverse sections showed that these crescents were built out of numerous small vesicles (arrow). (C, D) Rab8a colocalized with VatA at the collapsed CV bladder (arrowhead). (E) GFP-Sec15 and VatA localized to the same collapsed CV bladder (arrowhead), but GFP-Sec15 localized more peripherally than the VatA-positive CV bladder, likely because it is localized between PM and CV (arrows in magnification). All scale bars, 1 μm, except B, 5 μm.

fusion. We suggest that this exclusion zone around the fusion pore is the place of maximal tethering of the CV bladder to the PM. In *drainin*-null cells, this precise spatial arrangement was specifically altered. When exposed to hypo-osmotic medium they exhibit large, overinflated CV bladders tightly apposed to the PM, and both Rab8a and Sec15 localized to this broad area of contact (Figure 7, C–F, arrowheads). In extreme cases, Sec15 accumulated in an intensely stained and flat patch between the adjacent membranes (Figure 7, E and F), without forming "lips" around a fusion pore as was visible in Figures 3B and 4, E and F. We propose that Drainin is involved in restricting the activated Rab8a–exocyst complex to the CV bladder–PM contact zone and in the ensuing commitment to fusion pore formation.

LvsA promotes detethering of the CV bladder from the PM after discharge

GFP-LvsA localizes exclusively to the CV bladders in closest proximity to the PM (Figure 8A, arrowheads), and its arrival is coincidental with visible CV bladder contraction (Gerald *et al.*, 2002). The other bladders were often negative (Figure 8A, arrows). Exposure of *lvsA*-null cells to hypo-osmotic medium resulted in the disappearance of the CV reticulum. Instead, we observed CaM-positive CV structures collapsed against the PM, forming a hemispherical cap structure (Figure 8B) strongly reminiscent of the DD-GFP-Rab8a CA–induced phenotype. In both cases, numerous small CV-derived vesicles were docked beneath the PM (compare Figure 2, A and B, to Figure 8, B–E), indicative of postdischarge fragmentation of the CV, most probably by misfunctioning of the detethering and retrieval process from the PM. Despite this aberrant morphology, Rab8a and GFP-Sec15 colocalized with VatA at the collapsed CV vesicles

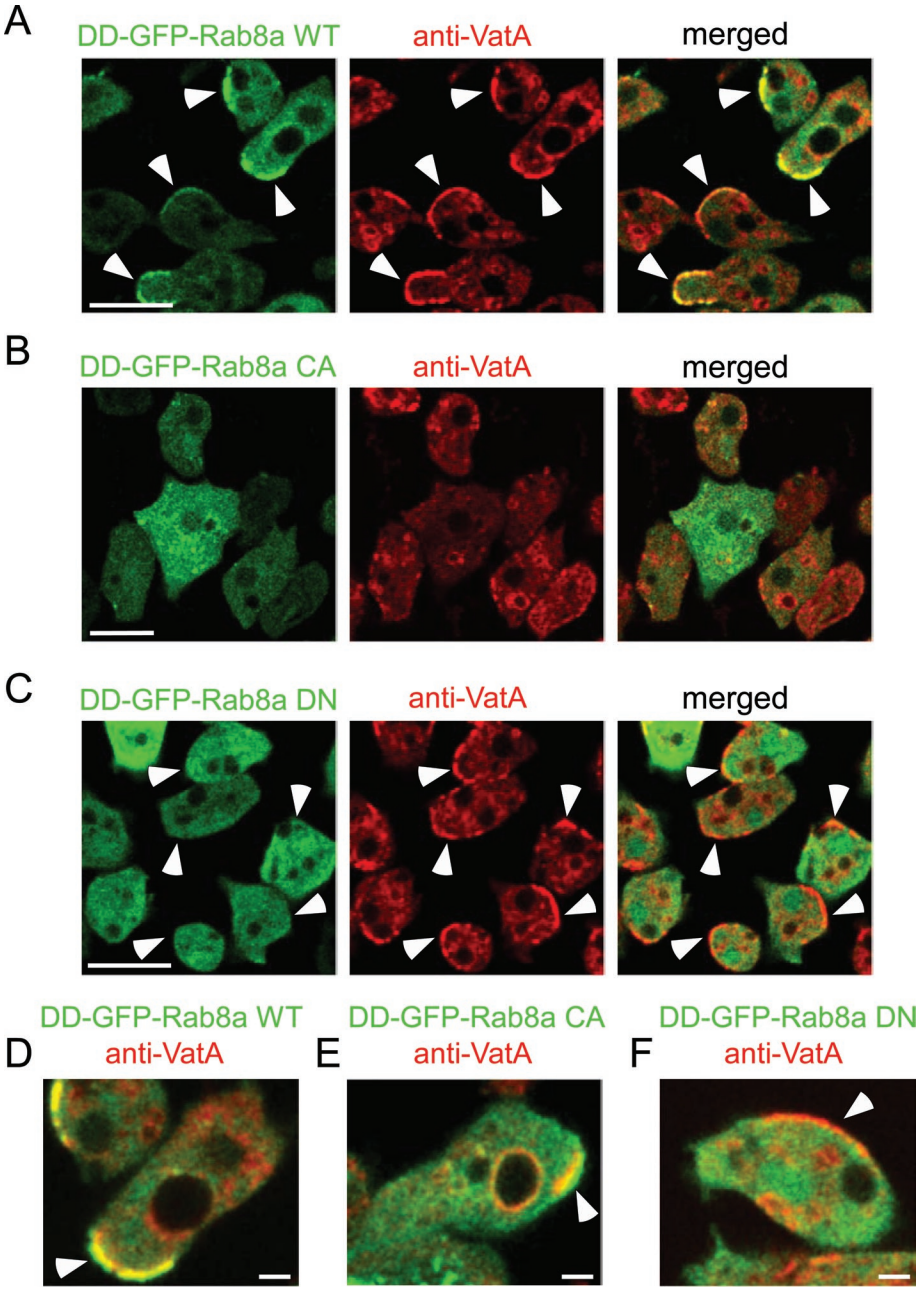

FIGURE 9: Expression of Rab8a CA reverts the CV phenotype of *lvsA*-null cells. *LvsA*-null cells overexpressing DD-GFP-Rab8a WT (A, D), CA (B, E), or DN (C, F) were treated as in Figure 1, fixed, and labeled for VatA. Single confocal sections at the middle of the cells are shown. DD-GFP-Rab8a WT colocalized at CV crescents (A, D, arrowheads), whereas DD-GFP-Rab8a DN remained cytosolic (C, F). Overexpression of both constructs had no effect on the *lvsA*-null phenotype, with most of the cells harboring a collapsed and fragmented CV (A, C, arrowheads). Overexpression of DD-GFP-Rab8a CA reversed the *lvsA*-null phenotype, with most cells showing a normal CV morphology (B). In the few cells where a CV crescent was visible, DD-GFP-Rab8a CA colocalized with VatA (E). Scale bars, 10 μm (A–C) and 2 μm (D– F).

(Figure 8, C–E). It is striking that detailed observations revealed that GFP-Sec15 localized more peripherally than VatA (Figure 8E, inset), consistent with Sec15 participating in the formation of a "picket fence/palisade" layer of proteins connecting the PM and the VatA-positive CV structure (Figure 8E). In wild-type cells, after completion of discharge, these connections are lost, detethered. This process is impaired in *lvsA*-null cells, indicating that LvsA is required for detethering. Considering that DD-GFP-Rab8a CA cells have a similar phenotype, we propose that joint action of LvsA and hydrolysis of GTP by Rab8a, possibly via the action of the Disgorgin GAP, is necessary for disassembly of the exocyst and release of the CV bladder.

In a previous report, a genetic interaction was identified between *LvsA* and *Disgorgin* (Du *et al.*, 2008). Therefore we tested the consequences of overexpressing various forms of Rab8a in *lvsA*-null cells. As shown in Figure 9, DD-GFP-Rab8a WT perfectly colocalized with VatA at collapsed and fragmented CV structures (Figure 9A), whereas DD-GFP-Rab8a DN remained cytosolic and did not affect the formation of the CV crescent (Figure 9C). In sharp contrast, expression of DD-GFP-Rab8a CA almost completely reversed the formation of the hemispherical CV cap induced by low osmolarity in *lvsA*-null cells (Figure 9B). Whereas in wild-type cells, both DD-GFP-Rab8a WT and CA localized to the CV (Supplemental Figure S1 and Figures 2 and 5), in *lvsA*-null cells, the CV localization of DD-GFP-Rab8a CA was greatly reduced but not abolished. In the few cells that showed some degree of collapsed CV, localization was visible (Figure 9E). In both cell types, DD-GFP-Rab8a WT is CV associated (Figure 9D), and DD-GFP-Rab8a DN did not localize to the CV (Figure 9F). These results suggests that an active CV discharge cycle is rescued by overexpression of DD-GFP-Rab8a CA in *lvsA*-null cells.

DISCUSSION

Exocytosis is a highly coordinated event of central importance in the homeostasis of cellular membranes. In this study, we report that the small GTPase Rab8a, together with the exocyst tethering complex, regulates the kiss-and-run exocytosis-like event of CV bladder discharge. We propose a detailed functional model (Figure 10) integrating our data with previous work in the field.

Before detailing the steps of our model, it is worth briefly mentioning that additional roles of the exocyst in *Dictyostelium* are likely because our unbiased Y2H screens revealed high-confidence binding partners involved in vesicle coat assembly, such as CopA (α-COP orthologue of the COP complex) and adaptor-related protein complex 1B (β-adaptin orthologue AP1B), members of the family of small GTPases such as Ras and ArfA (Arf1 orthologue), and some of their regulatory GEFs and GAPs. A potential role of the exocyst in post-Golgi traffic, as known for other organisms, was strengthened by the identification of the subunit CopB by IP/MS. Y2H revealed a large number of hits corresponding to a proteasome subunit, PsmD7. IP/MS confirmed the potential importance of this finding by identifying six other proteasome subunits (Supplemental Table S1C), as well as the ubiquitin UbqC fusion

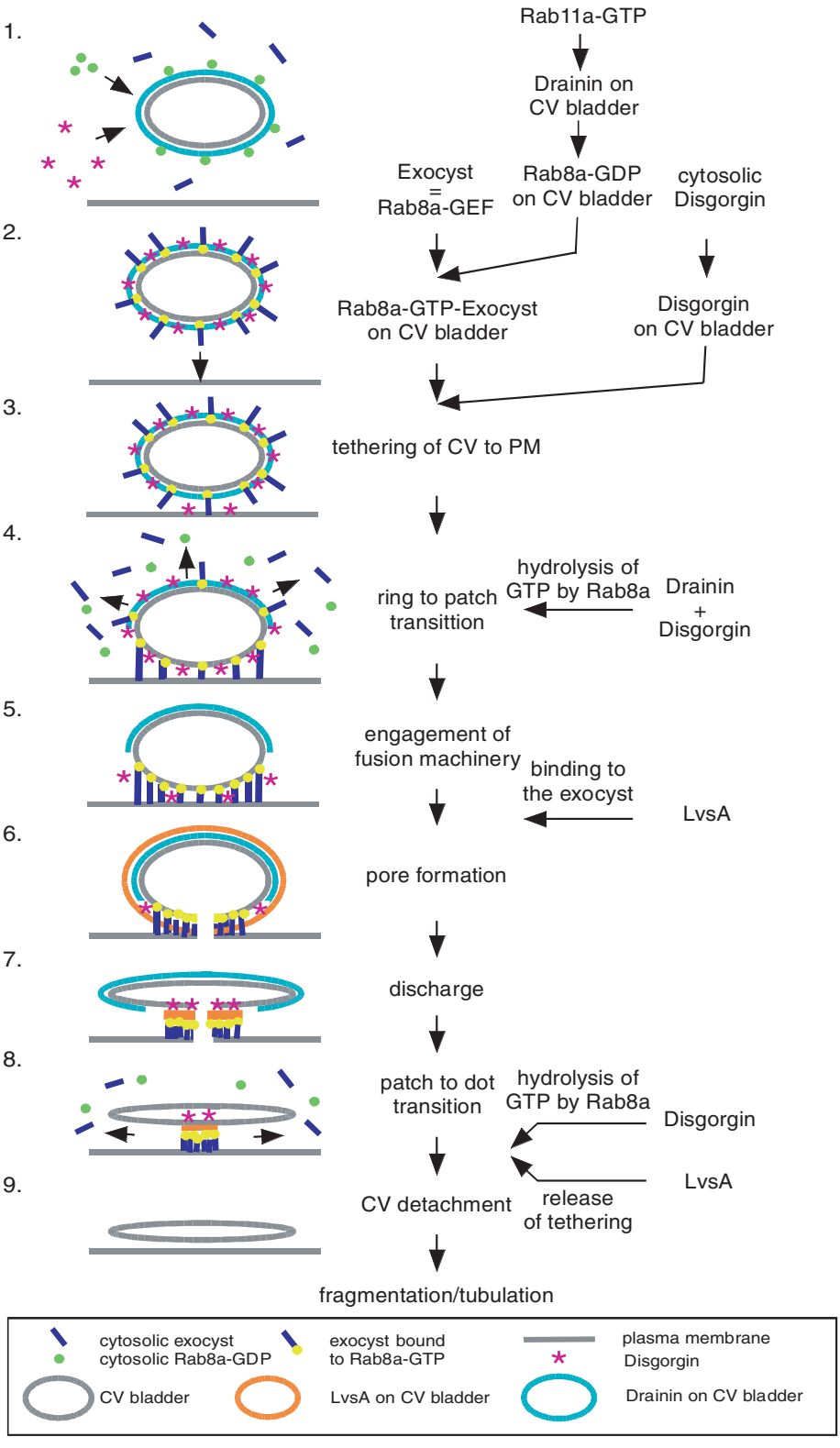

FIGURE 10: Schematic representation of the role of the proteins involved in the CV bladder discharge cycle. The flow diagram on the right gives additional information on the single steps. See the text for details.

protein. It is intriguing that UbqC and components of the SCF ubiquitination complex were reported to coIP with Disgorgin (Du *et al.*, 2008). Ubiquitination and proteasome fusion might be a final way to regulate disassembly and/or degradation of the complex.

Coming back to the model, we emphasize that the completion of a CV discharge cycle follows a precise sequence of events (Figure 10):

Step 1. In yeast, the Rab11 homologue, Ypt32p recruits Sec2, the Sec4-GEF, to the exocytic vesicle (Ortiz *et al.*, 2002). In *Dictyostelium*, Rab11a was proposed to be activated by a threshold of hypo-osmotic stress (Du *et al.*, 2008), and expression of Rab11a-DN induces enlarged CV bladders and renders cells osmosensitive (Harris *et al.*, 2001). We propose that Rab11a-GTP first recruits Drainin onto CV bladders (Du *et al.*, 2008), which, when the CV bladder reaches its maximal volume, in turn indirectly recruits Rab8a-GDP.

Step 2. Shortly afterward, the cytosolic exocyst complex is recruited to the CV concomitant with activation of Rab8a. Our data indicate that the GEF activity might be exerted by an unidentified exocyst-associated Rab8a-GEF or directly by one of the exocyst subunits, in analogy to the function of the Vsp39 subunit of the HOPS tethering complex, which directly activates Rab7 upon recruitment (Wurmser *et al.*, 2000). Disgorgin, a Rab8a-GAP, reaches the CV bladder at the same time by an independent mechanism (Du *et al.*, 2008).

Step 3. The CV bladder is translocated through and anchored at the actin cortex by the *Dictyostelium* type V myosin MyoJ for subsequent tethering. *MyoJ*-null cells show a strong accumulation of CV bladders in the cell center (Jung *et al.*, 2009).

In yeast, the mechanisms dictating the choice of the tethering place at the PM have been subjects of intense research. We propose the existence of two subcomplexes in *Dictyostelium*. One contains Sec3 and maybe Exo84, and the other one contains Sec15 plus Sec6, Sec8, Sec10, Exo70, and maybe Sec5. In analogy to the mammalian system, where Exo70 is targeted at the PM by the small GTPase TC10 (Inoue *et al.*, 2003), our data suggest a similar role for Rac1a in *Dictyostelium*. Rac1a is important for organization of the *Dictyostelium* actin cytoskeleton (Dumontier *et al.*, 2000), and knockout mutants of the Rac1a binding partner Rho-GDI1 show enlarged CV bladders (Rivero *et al.*, 2002). We speculate that Rac1a might have a Cdc42-like exocyst–PM targeting role (Adamo *et al.*, 2001; Zhang *et al.*, 2001) in the various exocytic pathways of *Dictyostelium*, but further functional studies might be hampered by the fact that Rac1a is functionally redundant with Rac1b and c (Chung *et al.*, 2000; Dumontier *et al.*, 2000; Palmieri *et al.*, 2000).

Steps 4–9. After exocyst tethering of the CV bladder at the PM, Drainin stimulates Disgorgin action, leading to dissociation of the

Rab8a-GDP exocyst complex from the CV bladder membrane (Step 4). Because Drainin is absent from the CV bladder–PM contact zone, the Rab8a-GTP–exocyst tethering complex remains and even concentrates (Step 5) at this interface. We observed this concentration during tethering of the CV bladder to the PM and pore formation as a progressive change in the localization of Rab8a and of the exocyst from a ring, to lips, to a dot structure (Steps 5–8). Analyses of *drainin*-null cells support this hypothesis. The CV bladders of *drainin*-null cells are broadly spread beneath the PM, and the two membranes are connected by a palisade-like structure (Becker *et al.*, 1999). We extend and strengthen this observation by localizing GFP-Sec15 in *drainin*-null cells, in which it is highly enriched in a large area between the CV bladder and the PM, suggesting that absence of Drainin-mediated enhancement of Disgorgin activity leads to uncontrolled accumulation of the exocyst tethers and a block in discharge. We suggest that these zones are the places of SNARE engagement (Step 5) and that Disgorgin-mediated concentration of Rab8a-GTP and the exocyst (Steps 3–5) is a prerequisite for pore formation (Step 6). Of interest, overexpression of Rab8a or Disgorgin rescues the *drainin*-null phenotype (Du *et al.*, 2008), showing that excess of Disgorgin might overcome the lack of activation by Drainin and allow pore formation. Following pore formation, the CV bladder undergoes discharge (Step 7). Despite the fact that in DD-GFP-Rab8a DN cells Rab8a cannot hydrolyze GTP, the cells are apparently still able to undergo CV discharge, even though the whole cycle is slowed down. We suggest that the Rab8a GDP/GTP cycle dictates the efficiency and timing of the entire process via the recruitment and regulation of the exocyst.

Finally, the collapsed CV bladder is detethered from the PM and reintegrated into the tubulovesicular CV system to start a new cycle of refill and discharge. Detethering seems to depend on the concerted action of Disgorgin and LvsA (Step 8). We propose that Sec15 recruits LvsA to the CV bladder as it reaches the PM. One function of LvsA might be to prevent homotypic fusion of CV bladders when preparing for pore formation and discharge. In the absence of LvsA in normal osmotic conditions, enlarged bladders are generated, in analogy to the *lvsB*-null phenotype characterized by enlarged lysosomes that might be caused by increased fusion (Harris *et al.*, 2002). A further possible function of LvsA could be in the detethering of the CV after discharge, because in *lvsA*-null cells under hypo-osmotic conditions, the collapsed vacuoles tethered to the PM fragment vanish, reminiscent of the *disgorgin*-null cell phenotype (Du *et al.*, 2008). In cells expressing DD-GFP-Rab8a CA, numerous small CV-derived vesicles also accumulate beneath the PM, but this phenotype is even more prominent than in *lvsA*-null and *disgorgin*-null cells because hydrolysis of GTP by Rab8a is completely blocked, whereas in the other mutants it likely happens with reduced uncatalyzed efficiency. We propose that hydrolysis of Rab8a-bound GTP by Disgorgin, together with a still-to-be-discovered biochemical activity of LvsA, is necessary for detethering from the PM (Steps 8 and 9).

Finally, our finding that expression of Rab8a CA reverts the collapsed and fragmented CV phenotype of *lvsA*-null cells is in perfect agreement with previously reported results (Du *et al.*, 2008). Indeed, it is logical that expression of Rab8a CA phenocopies the knockout of *Disgorgin*, the Rab8a GAP, which CV phenotype was shown to be rescued by further knockout of the *LvsA* gene. The Rab8a (Disgorgin)–LvsA genetic interaction corroborates the physical interaction reported here. How this complex behavior is performed at the biochemical level will be the topic of further studies and will shed light on the function of the still mysterious proteins of the Chédiak–Higashi family.

MATERIALS AND METHODS

Dictyostelium cell culture

The wild-type *Dictyostelium discoideum* strain Ax2 was cultivated axenically at 22°C in HL5c medium (ForMedium, Hunstanton, United Kingdom) supplemented with 10 U/ml penicillin and 10 µg/ml streptomycin (Life Technologies, Carlsbad, CA). The mutant strains were cultivated in the richer HL5 medium (14.3 g/l bactopeptone [L37; Oxoid, Basingstoke, United Kingdom], 7.15 g/l yeast extract, 18.0 g/l maltose monohydrate, 1.29 g/l $Na_2HPO_4 \times 12H_2O$, 0.49 g/l KH_2PO_4). The GFP and mRFP fusion protein constructs were expressed in the Ax2 background, selected, and maintained in 10 µg/ml G418 or 10 µg/ml blasticidin (Life Technologies) in HL5c, respectively. The *drainin*-null strain and the GFP-Drainin fusion construct were kind gifts of G. Gerisch (Max Planck Institute of Biochemistry, Martinsried, Germany; Becker *et al.*, 1999). The *lvsA*-null strain and the GFP-LvsA–expressing strain were kindly provided by A. DeLozanne (University of Texas, Austin, TX; Kwak *et al.*, 1999; Gerald *et al.*, 2002). The Q74L and N128I Rab8a mutant cDNAs were a kind gift of L. Temesvari (Clemson University, Clemson, SC; Powell and Temesvari, 2004). The Rab8a Q74L mutant is unable to hydrolyze GTP and therefore is constitutively active (CA). The Rab8a N128I mutant mimics the nucleotide-free form and therefore is dominant negative (DN).

Antibodies

The following antibodies were used: a mouse monoclonal antibody against the A subunit of the V-ATPase complex (VatA; monoclonal antibody, 221-35-2; Neuhaus *et al.*, 1998) and rabbit polyclonal antibodies against Dgap1 (Faix and Dittrich, 1996), Rhesus50 (Benghezal *et al.*, 2001), and calmodulin (Ulbricht and Soldati, 1999). The antibodies against mRFP, Sec3, and Rab8a were obtained during this study by immunization of rabbits with purified mRFP protein, purified GST-Sec3 N-terminus (amino acids [aa] 1–188), and a synthetic Rab8a peptide (aa 172–186: NH2-C-DIKKRMIDTPNEQPQ-CONH2). Commercial anti-GFP antibodies were used for immunoprecipitation (11 814 460 001, Roche, Indianapolis, IN; and GFP-Trap-A, ChromoTek (Martinsried, Germany), immunofluorescence, and immunoblot (598; MBL, Woburn, MA). As secondary antibodies for immunofluorescence, goat anti–mouse or goat anti–rabbit immunoglobulin G (IgG) coupled to Alexa 488 or Alexa 594 (Molecular Probes, Invitrogen, Carlsbad, CA) was used at a 1:2000 dilution. For immunoblots, goat anti–rabbit IgGs or goat anti–mouse IgGs conjugated to horseradish peroxidase (Bio-Rad, Hercules, CA) were used at dilutions between 1:2000 and 1:10,000.

Immunofluorescence

For immunofluorescence, cells on coverslips (grade 0; Hecht KG, Sondheim, Germany) were fixed by rapid freezing as described (Neuhaus *et al.*, 1998; Hagedorn *et al.*, 2006). The cells were plated on these coverslips the day before, exposed for 30 min to medium diluted 1:2 with water to enhance the activity of the contractile vacuole, and plunge-frozen. Then coverslips were transferred to phosphate-buffered saline (PBS) at room temperature and blocked by incubation in PBS containing 2% fetal bovine serum (FBS) for 10 min. PBS with 2% FBS was used for the antibody dilutions and washing steps. Cells were incubated with primary antibodies for 60 min, washed three times, and incubated with fluorescently labeled secondary antibodies and 4′,6-diamidino-2-phenylindole (1 µg/ml) for 60 min. After three washes, the slides were mounted in ProLong Antifade (Molecular Probes). Immunofluorescence samples were documented with a Leica SP2 confocal microscope (Leica, Wetzlar, Germany) using a 100×, 1.4 numerical aperture, oil immersion

objective. Recording parameters for fields of 1024 × 1024 pixels with appropriate electronic zoom (2–8×) were 4× line averaging and 0.1- to 0.32-μm vertical steps. Images and stacks were processed with ImageJ (National Institutes of Health, Bethesda, MD).

Live-cell imaging

For live-cell imaging, cells were transferred to 35-mm, optically clear plastic μ-Dish (Ibidi, Munich, Germany) with phosphate buffer (15 mM KH_2PO_4, 2 mM Na_2HPO_4, pH 6.0) and imaged immediately with a Leica AF6000 LX widefield microscope (frames were taken every second). To monitor the effect of the compound Shield-1 on the cells, they were imaged directly in the 12-well Petri dishes by phase-contrast or fluorescence microscopy using a Zeiss Axiophot 2 microscope with a 100× Achroplan water immersion objective (Carl Zeiss, Jena, Germany), and images were recorded with a charge-coupled device (CCD) camera (Imago Sensicam; PCO AG, Kelheim, Germany) and processed with ImageJ. For imaging with a spinning disk confocal microscope (Marianas SDC; Intelligent Imaging Innovations, Denver, CO; mounted on a Leica DMIRE2 inverted microscope), cells were plated on 35-mm μ-Dish at 30% confluence and incubated overnight in HL5c. At 1 h before imaging, the medium was replaced with low-fluorescence medium (LoFlo; ForMedium). Just before recording, LoFlo was replaced with LoFlo diluted 1:2 with water, and the cells were overlaid with a thin agar sheet (2% in water) as described (Yumura *et al.*, 1984). For TIRFM and IRCM, cells were plated onto glass coverslips (22 mm diameter, n_{546} = 1.5255, D263M; Menzel, Braunschweig, Germany) mounted in an Attofluor cell chamber (Invitrogen) and overlaid with ~1.5 ml of HL5c medium. The coverslip was precoated with 0.1% poly-L-lysine solution (Sigma-Aldrich, St. Louis, MO) for 5 min. For imaging, the chamber was mounted on a custom-built TIRFM based on an Olympus IX-70 body (Olympus, Hamburg, Germany) coupled with a Zeiss (100×, 1.45 numerical aperture) objective. Details of a similar TIRFM setup have been published (Merrifield *et al.*, 2005). The setup was further modified for IRCM by introducing widefield illumination from an amber (~594 nm, Luxeon K2; Philips Lumileds, San Jose, CA) light-emitting diode introduced into the light path via an 8:92 part-silvered pellicle (BP145B1; Thorlabs, Munich, Germany). The 488/568 DBX dichroic mirror had sufficient residual reflection at ~594 nm to allow IRCM. Custom timing electronics were fabricated to control the illumination mode using transistor–transistor logic (Radio Spares, Mörfelden-Walldorf, Germany) such that alternate TIRFM and IRCM images could be acquired. For simultaneous imaging of red and green fluorescence, an image splitter (Multispec Micro-Imager; Optical Insights, Santa Fe, NM) divided the red and green components of the images with a 565-nm dichroic mirror (Q565; Chroma, Brattleboro, VT) and passed the red component through a 585-nm longpass filter (585 nm AELP; Omega Optical, Brattleboro, VT) and the green component through a 525- to 575-nm bandpass filter (HQ525/50; Chroma). The images were then projected side by side onto a back-illuminated CCD camera (Cascade 512B; Roper Scientific, Ottobrunn, Germany). Each cell was imaged using MetaMorph (Molecular Devices, Sunnyvale, CA) for up to 18 min with 50- to 150-ms exposures at 1 Hz with TIRFM and IRCM alternated. For each acquisition session, an alignment image was acquired consisting of sparsely scattered 0.2-μm fluorescein isothiocyanate–conjugated beads (Molecular Probes). There was sufficient bleedthrough from green to red channels to image the beads in both the green and red channels, which thus provided fiducial markers in the *x*, *y* plane.

Immunoprecipitation

Two different protocols were applied. In protocol A, the anti-GFP antibody and protein G–Sepharose beads were added subsequently. In protocol B, a beads-coupled llama antibody was used.

Protocol A. A total of 2×10^7 cells were exposed for 30 min to medium diluted 1:2 with water, lysed in 600 μl lysis buffer (50 mM Tris, pH 7.5, 150 mM NaCl, 50 mM sucrose, 5 mM EDTA, 0.3% Triton X-100, complete protease inhibitors, 5 mM ATP, 1 mM GTPγS, 1 mM dithiothreitol), incubated on a rotating wheel at 4°C for 15 min, and centrifuged. For preclearing, 10 μl of a slurry of prewashed G Sepharose beads (G Sepharose 4B fast flow beads [Sigma-Aldrich]) were added to the lysate and incubated 30 min at 4°C on a rotating wheel and centrifuged. The supernatant was mixed with 6 μl of anti-GFP antibody and incubated 3 h on a rotating wheel at 4°C. Afterward, 30 μl of a slurry of G Sepharose beads were added, followed by a 5-h incubation on a rotating wheel at 4°C. Beads were washed twice with 500 μl of lysis buffer with Triton X-100 and three times with 500 μl of lysis buffer without Triton X-100 and taken up in 60 μl of SDS sample buffer for analysis on SDS–PAGE. As a negative control either a cell line expressing solely GFP or no GFP was used.

Protocol B. A total of 1×10^7 cells were exposed for 30 min to medium diluted 1:2 with water, lysed in 600 μl of lysis buffer (see earlier discussion), incubated on a rotating wheel at 4°C for 15 min, and centrifuged. The lysate was incubated with 25 μl of GFP-Trap-A (ChromoTek) for 2 h on a rotating wheel at 4°C. Beads were washed as described and taken up in 60 μl of SDS sample buffer for analysis on SDS–PAGE.

Silver stain and protein analysis by mass spectrometry analysis

Gel silver staining and protein analysis by mass spectrometry were performed exactly as described (Gotthardt *et al.*, 2006).

Analysis of mass spectrometry data

To analyze the raw mass spectrometry data, the following steps were undertaken. First, all the proteins that were identified in any lane, as well as in the negative control lanes, were ignored. Second, we used a stringent cutoff for identification and ignored all proteins falling under a Mascot score of 100, with the exception of proteins identified in multiple lanes and/or in the two screens, as, for example, ubqC or proteins that belong to complexes (exocyst, proteasome, and V-ATPase) and at least one subunit was above the threshold. These hits were, in screen 1, ap3b-1, nek2, nek3, exoc5, exoc7, vatD, vatM, vatE, psmD1, psmC4, psmC6, rac1A, ubqC, and dymB, and, in screen 2, psmC2, psmC4, psmC5, vatB, vatC, nek3, copB, and ubqC.

Immunoblots

Immunoblots were performed exactly as described (Gotthardt *et al.*, 2006).

Vector construction

For construction of the GFP and mRFP fusion proteins the full-length cDNAs were cloned into the vector pGEM T easy, sequenced, and then subcloned in the respective vectors, pDXA-GFP (Dieckmann *et al.*, 2010) or mRFPmars (Fischer *et al.*, 2004). The DD domain is a protein destabilization domain originally from the FK506- and rapamycin-binding protein (FKBP12). Fused to a protein of interest, it leads to immediate degradation of the fusion during or after translation. By addition of the compound Shield-1 the conformation of the DD domain is stabilized and protected from degradation (Banaszynski *et al.*, 2006). For construction of the DD-GFP-Rab8a vectors, the DD

domain was amplified by PCR from a plasmid (Herm-Gotz *et al.*, 2007) and cloned 5′ of the GFP sequence into pDXA-GFP. Then the sequences of Rab8a WT, CA, and DN (kindly provided by L. Temesvari, Clemson University; Powell and Temesvari, 2004) were inserted in-frame into the plasmid pDXA-DD-GFP.

ACKNOWLEDGMENTS

We thank Philippe Chavrier and Markus Maniak for significant input into the study and careful reading of the manuscript. We thank Thomas Ruppert and Armin Bosserhof for aiding in mass spectrometry, Francisco Rivero for performing preliminary experiments of binding of the exocyst to various Rac GTPases, and both F. Rivero and Hans Faix for expert advice on setting up GEF assays. The work was supported by the Swiss National Science Foundation.

REFERENCES

Adamo JE, Moskow JJ, Gladfelter AS, Viterbo D, Lew DJ, Brennwald PJ (2001). Yeast Cdc42 functions at a late step in exocytosis, specifically during polarized growth of the emerging bud. J Cell Biol 155, 581–592.

Banaszynski LA, Chen LC, Maynard-Smith LA, Ooi AG, Wandless TJ (2006). A rapid, reversible, and tunable method to regulate protein function in living cells using synthetic small molecules. Cell 126, 995–1004.

Becker M, Matzner M, Gerisch G (1999). Drainin required for membrane fusion of the contractile vacuole in *Dictyostelium* is the prototype of a protein family also represented in man. EMBO J 18, 3305–3316.

Benghezal M, Gotthardt D, Cornillon S, Cosson P (2001). Localization of the Rh50-like protein to the contractile vacuole in *Dictyostelium*. Immunogenetics 52, 284–288.

Blankenship JT, Fuller MT, Zallen JA (2007). The *Drosophila* homolog of the Exo84 exocyst subunit promotes apical epithelial identity. J Cell Sci 120, 3099–31.

Bos JL, Rehmann H, Wittinghofer A (2007). GEFs and GAPs: critical elements in the control of small G proteins. Cell 129, 865–877.

Boyd C, Hughes T, Pypaert M, Novick P (2004). Vesicles carry most exocyst subunits to exocytic sites marked by the remaining two subunits, Sec3p and Exo70p. J Cell Biol 167, 889–901.

Bush J, Nolta K, Rodriguez-Paris J, Kaufmann N, O'Halloran T, Ruscetti T, Temesvari L, Steck T, Cardelli J (1994). A Rab4-like GTPase in *Dictyostelium discoideum* colocalizes with V-H(+)-ATPases in reticular membranes of the contractile vacuole complex and in lysosomes. J Cell Sci 107, 2801–2812.

Bush J, Temesvari L, Rodriguez-Paris J, Buczynski G, Cardelli J (1996). A role for a Rab4-like GTPase in endocytosis and in regulation of contractile vacuole structure and function in *Dictyostelium discoideum*. Mol Biol Cell 7, 1623–1638.

Cascone I, Selimoglu R, Ozdemir C, Del Nery E, Yeaman C, White M, Camonis J (2008). Distinct roles of RalA and RalB in the progression of cytokinesis are supported by distinct RalGEFs. EMBO J 27, 2375–2387.

Charette SJ, Mercanti V, Letourneur F, Bennett N, Cosson P (2006). A role for adaptor protein-3 complex in the organization of the endocytic pathway in *Dictyostelium*. Traffic 7, 1528–1538.

Chen XW, Leto D, Chiang SH, Wang Q, Saltiel AR (2007). Activation of RalA is required for insulin-stimulated Glut4 trafficking to the plasma membrane via the exocyst and the motor protein Myo1c. Dev Cell 13, 391–404.

Chung CY, Lee S, Briscoe C, Ellsworth C, Firtel RA (2000). Role of Rac in controlling the actin cytoskeleton and chemotaxis in motile cells. Proc Natl Acad Sci USA 97, 5225–5230.

Dieckmann R *et al.* (2010). A myosin IK-Abp1-PakB circuit acts as a switch to regulate phagocytosis efficiency. Mol Biol Cell 21, 1505–1518.

Du F, Edwards K, Shen Z, Sun B, De Lozanne A, Briggs S, Firtel RA (2008). Regulation of contractile vacuole formation and activity in *Dictyostelium*. EMBO J 27, 2064–2076.

Duhon D, Cardelli J (2002). The regulation of phagosome maturation in *Dictyostelium*. J Muscle Res Cell Motil 23, 803–808.

Dumontier M, Hocht P, Mintert U, Faix J (2000). Rac1 GTPases control filopodia formation, cell motility, endocytosis, cytokinesis and development in *Dictyostelium*. J Cell Sci 113, 2253–2265.

Faix J, Dittrich W (1996). DGAP1, a homologue of rasGTPase activating proteins that controls growth, cytokinesis, and development in *Dictyostelium discoideum*. FEBS Lett 394, 251–257.

Fendrych M *et al.* (2010). The *Arabidopsis* exocyst complex is involved in cytokinesis and cell plate maturation. Plant Cell 22, 3053–3065.

Fischer M, Haase I, Simmeth E, Gerisch G, Muller-Taubenberger A (2004). A brilliant monomeric red fluorescent protein to visualize cytoskeleton dynamics in *Dictyostelium*. FEBS Lett 577, 227–232.

Gerald NJ, Siano M, De Lozanne A (2002). The *Dictyostelium* LvsA protein is localized on the contractile vacuole and is required for osmoregulation. Traffic 3, 50–60.

Gerisch G, Heuser J, Clarke M (2002). Tubular-vesicular transformation in the contractile vacuole system of *Dictyostelium*. Cell Biol Int 26, 845–852.

Gotthardt D, Blancheteau V, Bosserhoff A, Ruppert T, Delorenzi M, Soldati T (2006). Proteomics fingerprinting of phagosome maturation and evidence for the role of a Galpha during uptake. Mol Cell Proteomics 5, 2228–2243.

Gromley A, Yeaman C, Rosa J, Redick S, Chen CT, Mirabelle S, Guha M, Sillibourne J, Doxsey SJ (2005). Centriolin anchoring of exocyst and SNARE complexes at the midbody is required for secretory-vesicle-mediated abscission. Cell 123, 75–87.

Groves E, Dart AE, Covarelli V, Caron E (2008). Molecular mechanisms of phagocytic uptake in mammalian cells. Cell Mol Life Sci 65, 1957–1976.

Guo W, Roth D, Walch-Solimena C, Novick P (1999). The exocyst is an effector for Sec4p, targeting secretory vesicles to sites of exocytosis. EMBO J 18, 1071–1080.

Hagedorn M, Neuhaus EM, Soldati T (2006). Optimized fixation and immunofluorescence staining methods for *Dictyostelium* cells. Methods Mol Biol 346, 327–338.

Hala M *et al.* (2008). An exocyst complex functions in plant cell growth in *Arabidopsis* and tobacco. Plant Cell 20, 1330–1345.

Harata NC, Aravanis AM, Tsien RW (2006). Kiss-and-run and full-collapse fusion as modes of exo-endocytosis in neurosecretion. J Neurochem 97, 1546–1570.

Harris E, Wang N, Wu WL, Weatherford A, De Lozanne A, Cardelli J (2002). *Dictyostelium* LvsB mutants model the lysosomal defects associated with Chediak-Higashi syndrome. Mol Biol Cell 13, 656–669.

Harris E, Yoshida K, Cardelli J, Bush J (2001). Rab11-like GTPase associates with and regulates the structure and function of the contractile vacuole system in *Dictyostelium*. J Cell Sci 114, 3035–3045.

Hazuka CD, Foletti DL, Hsu SC, Kee Y, Hopf FW, Scheller RH (1999). The sec6/8 complex is located at neurite outgrowth and axonal synapse-assembly domains. J Neurosci 19, 1324–1334.

He B, Xi F, Zhang X, Zhang J, Guo W (2007). Exo70 interacts with phospholipids and mediates the targeting of the exocyst to the plasma membrane. EMBO J 26, 4053–4065.

Heath RJ, Insall RH (2008). *Dictyostelium* MEGAPs: F-BAR domain proteins that regulate motility and membrane tubulation in contractile vacuoles. J Cell Sci 121, 1054–1064.

Herm-Gotz A, Agop-Nersesian C, Munter S, Grimley JS, Wandless TJ, Frischknecht F, Meissner M (2007). Rapid control of protein level in the apicomplexan *Toxoplasma gondii*. Nat Methods 4, 1003–1005.

Heuser J (2006). Evidence for recycling of contractile vacuole membrane during osmoregulation in *Dictyostelium* amoebae—a tribute to Gunther Gerisch. Eur J Cell Biol 85, 859–871.

Heuser J, Zhu Q, Clarke M (1993). Proton pumps populate the contractile vacuoles of *Dictyostelium* amoebae. J Cell Biol 121, 1311–1327.

Hsu SC, Hazuka CD, Roth R, Foletti DL, Heuser J, Scheller RH (1998). Subunit composition, protein interactions, and structures of the mammalian brain sec6/8 complex and septin filaments. Neuron 20, 1111–1122.

Inoue M, Chang L, Hwang J, Chiang SH, Saltiel AR (2003). The exocyst complex is required for targeting of Glut4 to the plasma membrane by insulin. Nature 422, 629–633.

Jung G, Titus MA, Hammer JA 3rd (2009). The *Dictyostelium* type V myosin MyoJ is responsible for the cortical association and motility of contractile vacuole membranes. J Cell Biol 186, 555–570.

Kwak E, Gerald N, Larochelle DA, Vithalani KK, Niswonger ML, Maready M, De Lozanne A (1999). LvsA, a protein related to the mouse beige protein, is required for cytokinesis in *Dictyostelium*. Mol Biol Cell 10, 4429–4439.

Liu J, Zuo X, Yue P, Guo W (2007). Phosphatidylinositol 4,5-bisphosphate mediates the targeting of the exocyst to the plasma membrane for exocytosis in mammalian cells. Mol Biol Cell 18, 4483–4492.

Matern HT, Yeaman C, Nelson WJ, Scheller RH (2001). The Sec6/8 complex in mammalian cells: characterization of mammalian Sec3, subunit interactions, and expression of subunits in polarized cells. Proc Natl Acad Sci USA 98, 9648–9653.

Mellman I, Nelson WJ (2008). Coordinated protein sorting, targeting and distribution in polarized cells. Nat Rev Mol Cell Biol 9, 833–845.

Merrifield CJ, Perrais D, Zenisek D (2005). Coupling between clathrin-coated-pit invagination, cortactin recruitment, and membrane scission observed in live cells. Cell 121, 593–606.
Moskalenko S, Tong C, Rosse C, Mirey G, Formstecher E, Daviet L, Camonis J, White MA (2003). Ral GTPases regulate exocyst assembly through dual subunit interactions. J Biol Chem 278, 51743–51748.
Munson M, Novick P (2006). The exocyst defrocked, a framework of rods revealed. Nat Struct Mol Biol 13, 577–581.
Murthy M, Garza D, Scheller RH, Schwarz TL (2003). Mutations in the exocyst component Sec5 disrupt neuronal membrane traffic, but neurotransmitter release persists. Neuron 37, 433–447.
Myre MA, Lumsden AL, Thompson MN, Wasco W, Macdonald ME, Gusella JF (2011). Deficiency of huntingtin has pleiotropic effects in the social amoeba *Dictyostelium discoideum*. PLoS Genetics 7, e1002052.
Neuhaus EM, Almers W, Soldati T (2002). Morphology and dynamics of the endocytic pathway in *Dictyostelium discoideum*. Mol Biol Cell 13, 1390–1407.
Neuhaus EM, Horstmann H, Almers W, Maniak M, Soldati T (1998). Ethane-freezing/methanol-fixation of cell monolayers: a procedure for improved preservation of structure and antigenicity for light and electron microscopies. J Struct Biol 121, 326–342.
Ortiz D, Medkova M, Walch-Solimena C, Novick P (2002). Ypt32 recruits the Sec4p guanine nucleotide exchange factor, Sec2p, to secretory vesicles; evidence for a Rab cascade in yeast. J Cell Biol 157, 1005–1015.
Page LJ, Darmon AJ, Uellner R, Griffiths GM (1998). L is for lytic granules: lysosomes that kill. Biochim Biophys Acta 1401, 146–156.
Palmieri SJ, Nebl T, Pope RK, Seastone DJ, Lee E, Hinchcliffe EH, Sluder G, Knecht D, Cardelli J, Luna EJ (2000). Mutant Rac1B expression in *Dictyostelium*: effects on morphology, growth, endocytosis, development, and the actin cytoskeleton. Cell Motil Cytoskeleton 46, 285–304.
Powell RR, Temesvari LA (2004). Involvement of a Rab8-like protein of *Dictyostelium discoideum*, Sas1, in the formation of membrane extensions, secretion and adhesion during development. Microbiology 150, 2513–2525.
Reczek D, Bretscher A (2001). Identification of EPI64, a TBC/rabGAP domain-containing microvillar protein that binds to the first PDZ domain of EBP50 and E3KARP. J Cell Biol 153, 191–206.
Rivero F, Illenberger D, Somesh BP, Dislich H, Adam N, Meyer AK (2002). Defects in cytokinesis, actin reorganization and the contractile vacuole in cells deficient in RhoGDI. EMBO J 21, 4539–4549.
Rizzoli SO, Jahn R (2007). Kiss-and-run, collapse and "readily retrievable" vesicles. Traffic 8, 1137–1144.
Spiczka KS, Yeaman C (2008). Ral-regulated interaction between Sec5 and paxillin targets Exocyst to focal complexes during cell migration. J Cell Sci 121, 2880–2891.
Sztul E, Lupashin V (2009). Role of vesicle tethering factors in the ER-Golgi membrane traffic. FEBS Lett 583, 3770–3783.
Taheri-Talesh N, Horio T, Araujo-Bazan L, Dou X, Espeso EA, Penalva MA, Osmani SA, Oakley BR (2008). The tip growth apparatus of *Aspergillus nidulans*. Mol Biol Cell 19, 1439–1449.
TerBush DR, Novick P (1995). Sec6, Sec8, and Sec15 are components of a multisubunit complex which localizes to small bud tips in *Saccharomyces cerevisiae*. J Cell Biol 130, 299–312.
Tse FW, Iwata A, Almers W (1993). Membrane flux through the pore formed by a fusogenic viral envelope protein during cell fusion. J Cell Biol 121, 543–552.
Tsuboi T, Ravier MA, Xie H, Ewart MA, Gould GW, Baldwin SA, Rutter GA (2005). Mammalian exocyst complex is required for the docking step of insulin vesicle exocytosis. J Biol Chem 280, 25565–25570.
Ulbricht B, Soldati T (1999). Production of reagents and optimization of methods for studying calmodulin-binding proteins. Protein Expr Purif 15, 24–33.
Weeks G, Gaudet P, Insall H (2005). The small GTPase superfamily. In: *Dictyostelium* Genomics, ed. WF Loomis and A Kuspa, Norfolk, United Kingdom: Horizon Bioscience, 173–210.
Wu WI, Yajnik J, Siano M, De Lozanne A (2004). Structure-function analysis of the BEACH protein LvsA. Traffic 5, 346–355.
Wurmser AE, Sato TK, Emr SD (2000). New component of the vacuolar class C-Vps complex couples nucleotide exchange on the Ypt7 GTPase to SNARE-dependent docking and fusion. J Cell Biol 151, 551–562.
Yeaman C, Grindstaff KK, Nelson WJ (2004). Mechanism of recruiting Sec6/8 (exocyst) complex to the apical junctional complex during polarization of epithelial cells. J Cell Sci 117, 559–570.
Yumura S, Mori H, Fukui Y (1984). Localization of actin and myosin for the study of ameboid movement in *Dictyostelium* using improved immunofluorescence. J Cell Biol 99, 894–899.
Zanchi R, Howard G, Bretscher MS, Kay RR (2010). The exocytic gene secA is required for Dictyostelium cell motility and osmoregulation. J Cell Sci 123, 3226–3234.
Zhang X, Bi E, Novick P, Du L, Kozminski KG, Lipschutz JH, Guo W (2001). Cdc42 interacts with the exocyst and regulates polarized secretion. J Biol Chem 276, 46745–46750.
Zhang X, Orlando K, He B, Xi F, Zhang J, Zajac A, Guo W (2008). Membrane association and functional regulation of Sec3 by phospholipids and Cdc42. J Cell Biol 180, 145–158.
Zhang XM, Ellis S, Sriratana A, Mitchell CA, Rowe T (2004). Sec15 is an effector for the Rab11 GTPase in mammalian cells. J Biol Chem 279, 43027–43034.
Zhu Q, Clarke M (1992). Association of calmodulin and an unconventional myosin with the contractile vacuole complex of *Dictyostelium discoideum*. J Cell Biol 118, 347–358.
Zimmerberg J, Blumenthal R, Sarkar DP, Curran M, Morris SJ (1994). Restricted movement of lipid and aqueous dyes through pores formed by influenza hemagglutinin during cell fusion. J Cell Biol 127, 1885–1894.